Chapter 4
Theoretical Aspects of Polymer Crystallization

Wenbing Hu and Liyun Zha

4.1 Introduction

A vast amount of natural and synthetic polymers are semicrystalline. From this standpoint alone, it is necessary to understand the process of polymer crystallization, which dominates the structure formation of semicrystalline polymers and thus allows us to control their morphologies and properties. Polymer crystallization is influenced by many factors, such as chemical structures, compositions, temperatures, and thermal history. The theoretical models serve as a powerful tool for us to comprehend these factors in polymer crystallization.

Thermodynamics and kinetics are the two most fundamental theoretical aspects of polymer crystallization. Thermodynamics addresses why, or under which circumstances, polymer crystallization will begin, or in the opposite direction polymer crystals will start to melt. Kinetics addresses how fast polymer crystallization will be initiated, be developed, and be further improved. Both aspects decide crystal morphologies that eventually influence the properties of polymer materials.

This chapter intends to make a brief survey on our current theoretical understanding about the basic thermodynamics and kinetics of polymer crystallization. On thermodynamics, we will introduce the melting point, metastable states, phase diagrams, mesophase formation, as well as those factors governing melting points. On this aspect, the mean-field lattice theory on the statistical thermodynamics of crystallizable polymer solutions will be focused. On kinetics, we will introduce the basic knowledge about crystal nucleation, crystal growth, and crystal annealing. On this aspect, the classical nucleation theory and the related kinetic equations will be focused.

W. Hu (✉) • L. Zha
School of Chemistry and Chemical Engineering, Nanjing University, Nanjing 210023, China
e-mail: wbhu@nju.edu.cn

G.R. Mitchell, A. Tojeira (eds.), *Controlling the Morphology of Polymers*,
DOI 10.1007/978-3-319-39322-3_4

Due to length limitation of this chapter, many theoretical approaches on the phenomenological aspects of polymer crystallization have to be skipped. The isothermal and non-isothermal kinetic analysis of overall crystallization appears as technically important in the data treatment of DSC measurements. Some theoretical considerations on the metastable aspects of crystal morphologies and their evolution under various circumstances appear as practically important and case sensitive (see Chap. 1). In this sense, a combination of this chapter with other contributions of this book will provide reader a broad cutting-edge knowledge about our basic understanding of polymer crystallization.

4.2 Thermodynamics of Polymer Crystallization

4.2.1 Basic Concepts

Polymers are either in the fully amorphous state or in the fully crystalline state, or in the states partial between them. When they are in the amorphous state of homogeneous solutions or melt, polymer chains are fully disordered, as described by a random-coil model. The random-coil model was first proposed by Kuhn (1934) as well as by Guth and Mark (1934) to predict the entropic elasticity of polymer chains, and then was used to describe the amorphous state of polymers by Flory (1953) and others.

Polymer crystallization and melting are typically first-order phase transitions between the amorphous phase and the crystalline phase. When these two phases are in thermodynamic equilibrium, two phase transitions are thermodynamically reversible under a certain temperature. This temperature is referred to the equilibrium melting point of polymer crystallization. The free energy changes of amorphous phase and crystalline phase under various temperatures are depicted in Fig. 4.1, illustrating the definition of the equilibrium melting point T_m^0.

In the bulk system of pure polymers, the free energy change of melting becomes zero when the system is under its equilibrium melting point, as given by

$$\Delta F_m = \Delta Q_m - T_m^0 \Delta S_m = 0 \tag{4.1}$$

The equilibrium melting point can accordingly be calculated by

$$T_m^0 = \Delta Q_m / \Delta S_m \tag{4.2}$$

In practice, to get over the nucleation barrier via thermal fluctuations, the initiation of primary crystal nucleation requires a crystallization temperature T_c something lower than T_m^0, and thus a supercooling for crystallization is defined as

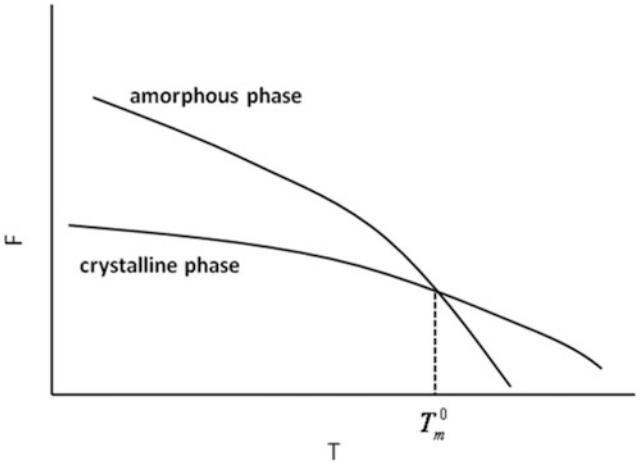

Fig. 4.1 Schematic free energy curves of amorphous phase and crystalline phase versus temperature. The temperature at which two curves intersect with each other is defined as the equilibrium melting point of polymers

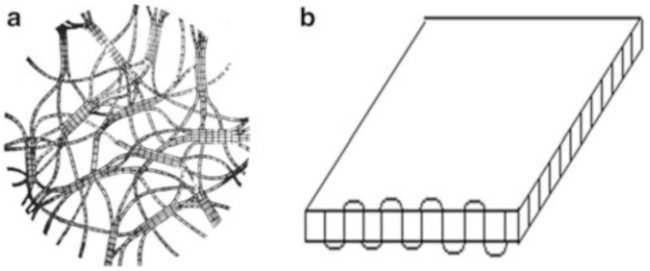

Fig. 4.2 Illustration pictures on the models of (**a**) fringed-micelle (Hermann et al. 1930) and (**b**) adjacent chain-folding (Keller 1957)

$$\Delta T = T_{\mathrm{m}}^{0} - T_{\mathrm{c}} \tag{4.3}$$

In order to overcome the kinetic barrier under a certain supercooling, polymer crystallization commonly chooses a pathway favoring its kinetics, which will result in metastable semicrystalline states (Cheng 2008). It took a long time for people to figure out the structure features of the metastable semicrystalline polymers, with two dominant models, i.e., fringed-micelle and chain-folding models, as illustrated in Fig. 4.2. Here, the metastable state holds either a thermodynamic meaning as its local minimum in the free energy landscape, or a dynamic meaning with its negligible changes over the time window of our observations upon a very slow evolution towards more stable states.

In 1930, Hermann et al. set up the fringed-micelle model (Hermann et al. 1930; Hermann and Gerngross 1932) to describe the high elasticity of low-density

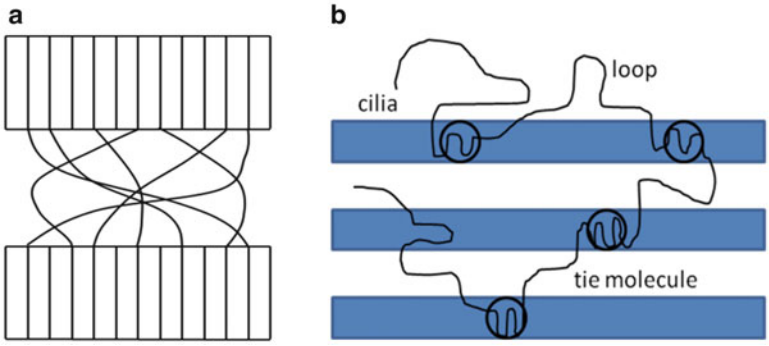

Fig. 4.3 Illustration pictures on the models of (**a**) Switchboard (Flory 1962) and (**b**) variable clusters (Hoffman 1983)

polyethylene products. But later on, this model could not explain the spherulite morphologies of polymer crystals often observed under optical microscopy. In 1957, Keller set up the adjacent chain-folding model (Keller 1957) on the basis of the facts that polymer stems in single lamellar crystal grown from dilute solutions were perpendicular to the lamellar surface, and the lamellar thickness was only in the scale of one tenth of chain lengths. This model was then confirmed by the small-angle neutron scattering (SANS) experiments of single crystal grown in dilute solutions (Spells et al. 1980) as well as by the integer folding of short chains in lamellar crystals grown in the melt (Arlie et al. 1966, 1967; Ungar et al. 1985; Organ and Keller 1987). For lamellar crystals grown in the long-chain melt, Flory proposed the "Switchboard" model (Flory 1962), which was then developed into the interzonal Switchboard model as discussed by Mandelkern (1964). Since both adjacent chain-folding and Switchboard models have their own interpretations on the same SANS experiment data, there was a hot debate in 68th Faraday Discussion Meeting. It is now well accepted that either model describes a certain aspect of structural features on lamellar crystals grown in the melt. The variable cluster model synthesizing both features of local chain-folding and global random-coil was discussed by Hoffman (1983). The loops, cilia, and tie molecules (Fig. 4.3) are restricted at the fold-end surfaces of lamellar crystals, which constitute the rigid amorphous phase near the crystalline region. The latter pretends to be the third phase besides the mobile amorphous phase and the crystalline phase, and appears as important in the thermal and mechanical properties of semicrystalline polymers (Wunderlich 2003).

As will be introduced in the following kinetic aspects of polymer crystallization, secondary intramolecular crystal nucleation favors chain-folding upon crystal growth, which dominates the lamellar feature of crystal morphologies. The metastable lamellar crystals intend to perform thickening into a more thermodynamically stable state upon annealing. Before they are able to reach the most stable state, their melting points appear as lower than the equilibrium melting point of infinitely large crystals. This is mainly because of a limited dimension in lamellar thickness.

The lowered melting point of lamellar crystals T_m is described by the well-known Gibbs–Thomson equation, as given by

$$T_m = T_m^0 - \frac{2\sigma_e T_m^0}{l\Delta h} \tag{4.4}$$

where σ_e is the free energy density of the fold-end surface, l is the lamellar thickness, and Δh is the heat of fusion.

A wide distribution of lamellar thickness in polymer crystals results in a broad range of melting temperature, shown as a wide melting peak in the heating curve of differential scanning calorimetry (DSC). We pragmatically define the peak temperature as the experimentally observed melting point of polymer crystals, which could be far below the equilibrium melting point due to the limited lamellar thickness.

Crystallization under various temperatures yields different corresponding lamellar thicknesses, exhibiting different variable melting points. This phenomenon allows us to derive the equilibrium melting point at the infinitely large crystal according to the Gibbs–Thomson equation, provided that there is no annealing effect upon heating the crystals for the measurement of their melting points. However, most of metastable crystals do perform annealing behaviors upon heating towards melting. Hoffman and Weeks (1965) supposed that lamellar crystals will thicken into a metastable state with the thickness several times larger than the minimum thickness, and derived the equilibrium melting point as the crossover point of the extrapolated T_m versus T_c curve at $T_m = T_c$. Although the fixed folds of thickness increase appear as a big assumption, this method has been widely applied to derive the equilibrium melting points of various semicrystalline polymers in the literature.

Besides crystallization, liquid–liquid (L–L) demixing is another basic phase transition in polymer solutions, and both of them are functions of polymer concentrations and temperatures. The schematic L–L binodal and liquid–solid (L–S) coexistence curves in polymer solutions are separately shown in Fig. 4.4. The

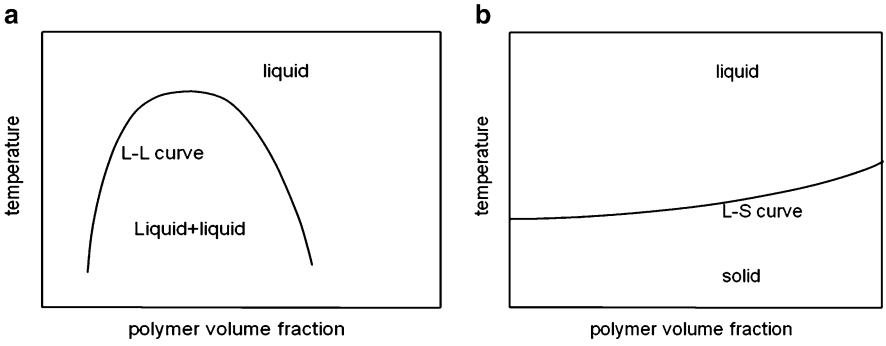

Fig. 4.4 Schematic pictures of (**a**) L–L binodal curve and (**b**) L–S coexistence curve in polymer solutions

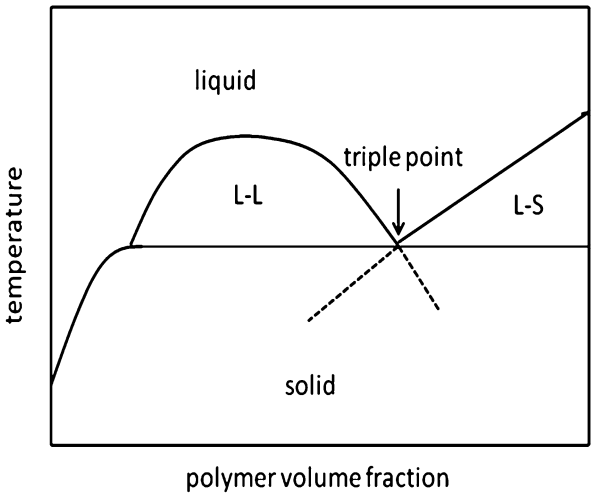

Fig. 4.5 Schematic picture of typical phase diagrams combining both L–L binodal and L–S coexistence curves in polymer solutions

illustrated L–L binodal contains an upper critical solution temperature. Some solution binodals may contain a lower critical solution temperature, or even both.

When the L–S curve intersects with the L–L curve in the overlapping temperature windows, both curves will be terminated at the intersection point, which is referred to the monotectic triple point. The typical phase diagram in polymer solutions is shown in Fig. 4.5.

In between the amorphous phase and the crystalline phase, there sometimes occurs an important intermediate phase for polymers carrying anisotropic groups (called mesogen groups) either on the chain backbone or on the chain branches, which is referred to mesophase. The mesogen groups become orientational-ordered under suitable thermodynamic conditions. This ordered state could be the well-known liquid crystal (LC) state, as a typical mesomorphic state between the amorphous state and the crystalline-ordered state for LC polymers.

The transition temperature from LC mesophase to melt is often named as the clearing point or the isotropization point T_i. If the LC mesophase is thermodynamically stable, it will occur in both heating and cooling curves when detected by DSC measurements. This mesophase is also referred to the enantiotropic mesophase. If the mesophase is kinetically favored due to large supercooling required for the initiation of crystallization, it will occur only in the cooling curve but not in the heating curve. This mesophase is then referred to the monotropic mesophase. The free energy plots for the two kinds of mesophases are demonstrated in Fig. 4.6.

When L–S phase transition is accompanied by LC transition, the above phase diagram of polymer solution becomes more complicated as illustrated in Fig. 4.7.

According to the phase diagram schematically shown in Fig. 4.7, two types of liquid crystal ordering with different preparation methods can be categorized. One is the lyotropic liquid crystal approached by changing the concentration in solutions. The other is the thermotropic liquid crystal approached by changing the

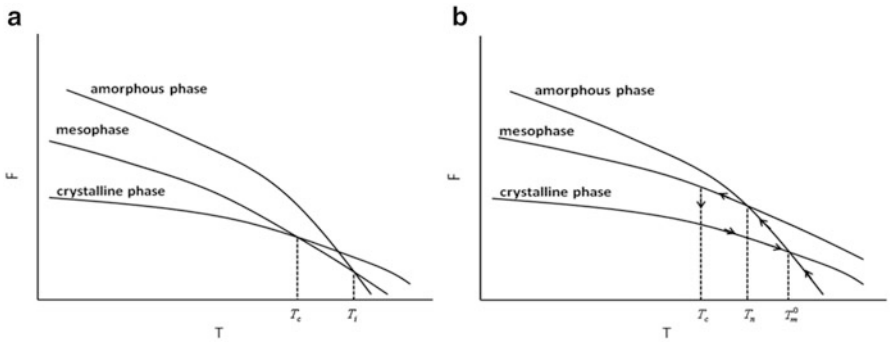

Fig. 4.6 Schematic pictures of (**a**) enantiotropic mesophase and (**b**) monotropic mesophase

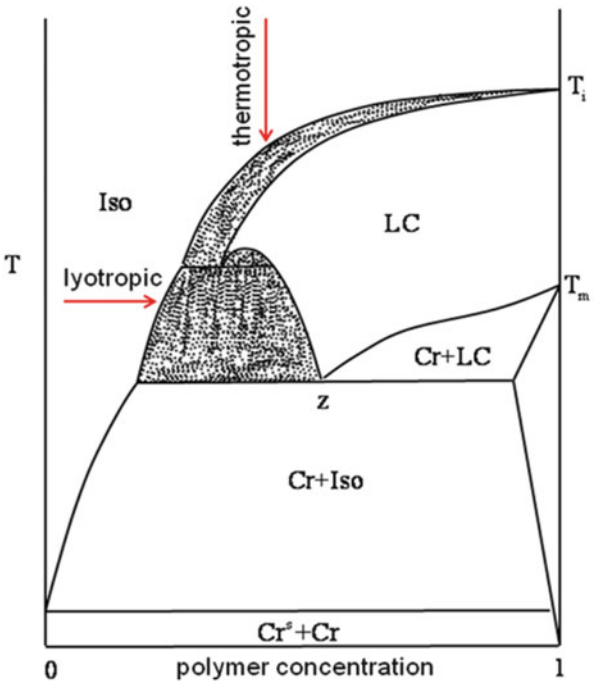

Fig. 4.7 Schematic picture of typical phase diagram of polymer solutions combining L–L binodal (Iso), L–S coexistence (Cr), and L-liquid crystal-S coexistences (LC). The two *arrows* in the picture show the preparation methods of thermotropic liquid crystal and lyotropic liquid crystal, respectively (Keller 1992)

temperature in the concentrated solutions or in the bulk phase. Their conventional preparation methods are schematically shown in Fig. 4.7. According to Onsager's interpretation (Onsager 1949), the lyotropic liquid crystal results from an entropy-driven phase transition due to anisotropic excluded-volume interactions of mesogens. When the concentration of rod-like molecules becomes high enough, the space for anisotropic particles to move freely appears limited, resulting in an entropic loss. In this case, if parts of rodlike particles are aligned in parallel with each other in a domain of higher concentration, they release part of their space for

the movement of other particles and thus increase the total entropy. This entropy-driven phase transition makes the ordered system stable. For the thermotropic liquid crystal, Maier and Saupe's theory (1959) considers that the thermotropic liquid crystal is a result of orientation-dependent dispersion interactions between mesogens. With the decrease of temperature, spontaneous orientational ordering lowers the attractive potential energy. Combination of the above two theories gave a better interpretation to the orientational ordering for the formation of liquid crystals as well as a better calculation of phase diagrams (Jähnig 1979; Ronca and Yoon 1982, 1984; ten Bosch et al. 1983a, b; Khokhlov and Semenov 1985; Gupta and Edwards 1993; Lekkerkerker and Vroege 1993).

4.2.2 *Statistical Thermodynamics of Polymer Crystallization*

Statistical thermodynamic theories provide a powerful tool to bridge between the microscopic chemical structures and the macroscopic properties. Lattice models have been widely used to describe the solution systems (Prigogine 1957). Chang (1939) and Meyer (1939) reported the earliest work related with the lattice model of polymer solution. The lattice model was then successfully established by Flory (1941, 1942) and Huggins (1942) to deal with the solutions of flexible polymers by using a mean-field approximation, and to derive the well-known Flory–Huggins equation.

In the lattice model of polymer solutions, polymer chain is simply represented by a number of consecutively occupied lattice sites, each site corresponding to one chain unit. The rest single sites are assigned to solvents. This simple lattice treatment of polymer solutions allows a very convenient way to calculate thermodynamic properties of flexible and semiflexible polymer solutions from the statistical thermodynamic approach. By the mean-field assumption, the entropy part and the enthalpy part of partition function can be separately calculated.

Following Flory's treatment of semiflexible polymer solutions (Flory 1956), the entropy part of partition function for polymer solutions is given by

$$Z_{\text{comb}} \approx \left(\frac{n}{n_1}\right)^{n_1} \left(\frac{n}{n_2}\right)^{n_2} \left(\frac{q z_{\text{c}}^{r-2}}{2e^{r-1}}\right)^{n_2} \tag{4.5}$$

where n_1 is the number of solvent molecules, n_2 is the number of polymer chains, each chain composed of r monomers, and $n = n_1 + n_2 r$ is the total lattice sites occupied by solvent and polymer chains. q is the coordination number of the lattice space. z_{c} is the conformational partition function defined as

$$z_{\text{c}} = 1 + (q-2)\exp\left(-\frac{E_{\text{c}}}{kT}\right) \tag{4.6}$$

where E_c is the energy penalty for the $q-2$ noncollinear consecutive bonds along the polymer chain with a reference to the collinear connection, k is Boltzmann constant, and T is system temperature.

The partition function related with the mixing enthalpy of solvent and monomers is given by

$$z_m = \exp\left[-(q-2)\frac{n_1}{n} \times \frac{B}{kT}\right] \tag{4.7}$$

where B is the energy change for a pair of solvent and monomer before and after mixing as defined by

$$B = E_{12} - \frac{E_{11} + E_{12}}{2} \tag{4.8}$$

As polymer crystals are commonly featured with parallel packing of polymer chains, the driving force for crystallization can be modeled as the parallel packing of bonds in the lattice model (Hu 2000). Assuming the energy penalty for nonparallel packing of two bonds is E_p, deviating from the ground state with parallel-packed bonds, the partition function related to nonparallel packing of neighboring bonds around a chain bond is given by Hu and Frenkel (2005)

$$z_p = \exp\left\{-\frac{q-2}{2}\left[1 - \frac{2(r-1)n_2}{qn}\right]\frac{E_p}{kT}\right\} \tag{4.9}$$

Thus after integrating different parts, the total partition function of polymer solutions can be described as

$$Z = \left(\frac{n}{n_1}\right)^{n_1}\left(\frac{n}{n_2}\right)^{n_2}\left(\frac{q}{2}\right)^{n_2} e^{-(r-1)n_2} z_c^{(r-2)n_2} z_m^{rn_2} z_p^{(r-1)n_2} \tag{4.10}$$

The corresponding free energy density is calculated according to Boltzman's relationship, as given by

$$\begin{aligned}\frac{f(\phi)}{k_B T} = {} & (1-\phi)\ln(1-\phi) + \frac{\phi}{r}\ln\phi \\ & + \phi\left(-\frac{\ln(qr/2)}{r} - (1-2/r)\ln z_c + (1-1/r) + (q-2)\frac{B}{k_B T} + (1-1/r)\frac{q-2}{2}\frac{E_p}{k_B T}\right) \\ & - \phi^2\left((q-2)\frac{B}{k_B T} + (1-1/r)^2\frac{q-2}{q}\frac{E_p}{k_B T}\right)\end{aligned} \tag{4.11}$$

Equation (4.11) can be used to calculate various thermodynamic properties of polymers, in particular, the equilibrium melting point. It can be used to calculate the mixing free energy and the binodal L–L curve, as well as the coexistence L–S curve in polymer solutions.

Following the protocols of molecular interactions set up in the lattice statistical thermodynamic theory introduced above, Monte Carlo simulations appear as a powerful tool in the study of both thermodynamics and kinetics of polymer crystallization (Hu and Frenkel 2005). Polymer motions in the simulations can be realized by a micro-relaxation model (Hu 1998). Its acceptance is judged by the Metropolis importance sampling algorithm (Metropolis et al. 1953), with the potential energy change in each step of micro-relaxation composed of three contributions, noncollinear connections of consecutive bonds along polymer chains (E_c) (Flory 1956), mixed pairs of polymer monomer and solvent (B) (Flory 1942; Huggins 1942), and nonparallel packing of neighboring bonds (E_p) (Hu 2000). The micro-relaxation model is highly efficient in relaxing local chain conformation and is a suitable approach for the study of polymer crystallization. Results from Monte Carlo simulations will be introduced along with theories of polymer crystallization in the following paragraphs.

4.2.3 Properties of Equilibrium Melting Points

4.2.3.1 Interaction Parameters

Although a precise measurement of the equilibrium melting point appears as a big challenge to the practical experiments, the statistical thermodynamic theory can predict equilibrium melting point on the basis of the mean-field assumption. Taking the fully ordered extended chains as the ground state, and considering bulk polymers with infinitely long polymer chains, $r \to \infty$, $n_1 = 0$, $n = rn_2$, one can get the free energy of the amorphous state from (4.11),

$$\frac{F}{nkT} = 1 - \ln z_c + \frac{(q-2)^2}{2q} \times \frac{E_p}{kT} \tag{4.12}$$

At the equilibrium melting point, the free energy of the amorphous state is equal to that of the ground crystalline state (zero), so inserting the expression of z_c, one can derive

$$1 + (q-2)\exp\left(-\frac{E_c}{kT_m}\right) = \exp\left[1 + \frac{(q-2)^2}{2q} \times \frac{E_p}{kT_m}\right] \tag{4.13}$$

Supposing that the first term "1" in the left-hand side of the equation is relatively small, one can omit it and derives the equilibrium melting point of bulk polymers, as given by

$$T_m \approx \frac{E_c + \frac{(q-2)^2}{2q}E_p}{k\ln(q-2) - k} \tag{4.14}$$

From (4.14), we can clearly see that a larger E_c (a higher rigidity of polymer chains) favors a higher equilibrium melting point. For polyolefins, larger substitute groups benefit their higher melting points because internal rotation of polymer chains becomes more difficult. For instance, the melting point of polyethylene (–($–CH_2CH_2)_n$–) is 146 °C, the melting point of polypropylene (–(–$CH_2CH(CH_3)$)$_n$–) is 187 °C while for poly-3-methyl-1-butene (–(–$CH_2CH(CH(CH_3)_2)$)$_n$–), its melting point is 304 °C. Apparently, more rigid groups on the backbones benefit their higher melting point as well. For instance, the melting point of polyethylene (–($–CH_2CH_2)_n$–) is 146 °C, while with increasing benzene-ring density on the polymer chains the melting point of poly-p-xylene (–($–CH_2–\phi–CH_2–)_n$–) is 375 °C and that of polyphenylene (–($–\phi–)_n$–) is as high as 530 °C. Another example, the melting point of polyethylene adipate (–($CH_2CH_2–OCO–C_6H_{12}–OCO)_n$–) is 52 °C, while the melting point of polyethylene terephthalate (–($CH_2CH_2–OCO–\phi–OCO)_n$–) is 265 °C, and that of polyethylene naphthalene-2,6-dicarbonoxylate (–($CH_2CH_2–OCO–\phi–\phi–OCO)_n$–) reaches the highest 355 °C. Melting point of polymers with extremely high rigidity may be even higher than their thermal degradation temperature where their melt phase cannot be reached. On the other hand, a larger E_p favors also a higher equilibrium melting point. Longer side groups do not help the compact packing of backbone chains. Taking the melting points of (CH_2-CHR)$_n$ for example, if R group represents –CH_3, –CH_2CH_3, –$CH_2CH_2CH_3$, and –$CH_2CH_2CH_2CH_3$, respectively, the corresponding melting points are 187 °C, 138 °C, 130 °C, and −55 °C, respectively. The larger polarity of side groups also benefits the higher melting point of polymers. For instance, the melting point of polyethylene (–($–CH_2CH_2)_n$–) is 146 °C, while the melting point of polyvinyl chloride (–($–CH_2CHCl)_n$–) is 227 °C and that of polyacrylonitrile (–($–CH_2CHCN)_n$–) is 265 °C. In the last case, the sequence regularity becomes a minor factor for the capability of crystallization.

The linear relationship between the melting points and E_p/E_c values in (4.14) is further confirmed by Monte Carlo simulations of polymers, and the results are shown in Fig. 4.8. The high consistency in the results between the lattice theory and Monte Carlo simulations validates the mean-field treatment in the lattice theory of polymer solutions.

4.2.3.2 Molecular Weights

In the equilibrium states of polymer crystals, the chain ends can be regarded as the crystalline defects in the infinitely large crystals formed by extended chains, which will apparently result in a depression of melting points with the increase of concentrations of chain ends, or in other words, with the decrease of chain lengths.

In the calculation of melting point of polymers with different molecular weights, Flory and Vrij (1963) divided the free energy change of melting into three parts. The first part is the free energy change for the melting of infinitely long polymers, the second part is the free energy change by introducing chain-end defects in the crystals, and the third part is the conformational entropy change when the infinitely

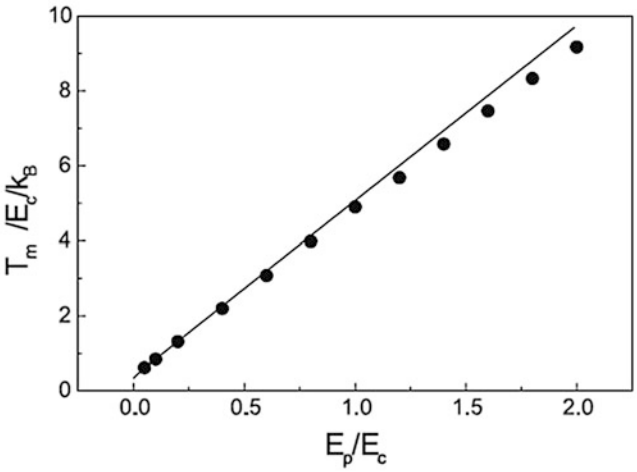

Fig. 4.8 Melting temperature ($T_m/E_c/k_B$) of bulk polymers with variable E_p/E_c values. *The Solid line* is calculated from (4.13) and the *circles* are simulation results of 32-mer polymer solutions with a concentration of 0.9375 in a 32^3 cubic lattice (Hu and Frenkel 2005)

long polymer chain is cut into the segments with limited chain length r. So the total free energy change of melting can be described as

$$\Delta F_m = r\Delta F_u + \Delta F_e - kT_m \ln r = 0 \tag{4.15}$$

ΔF_u is the free energy change of fusion, it can be calculated by

$$\begin{aligned} \Delta F_u &= \Delta h_u - T_m \Delta s_u \\ &= E_c + \frac{(q-2)^2}{2q} E_p - k_B T_m [\ln(q-2) - 1] \end{aligned} \tag{4.16}$$

ΔF_e is the extra free energy change due to the existence of chain ends, which can be calculated from the equilibrium condition $f = 0$ in (4.11) by setting the chain length $r = 2$ in the melt phase.

$$\Delta F_e = \frac{(q-2)(q-1)}{2q} E_p - k_B T_m (\ln q - 1) - 2\Delta f_u \tag{4.17}$$

The term $\ln(r)$ represents a change of conformational entropy upon cutting. Inserting (4.16) and (4.17) into (4.15), the equilibrium melting point predicted by the Flory–Vrij theory can be calculated.

One can also directly calculate the equilibrium melting point from (4.11). Under equilibrium melting temperature,

$$\mu^c = \mu^s \tag{4.18}$$

where μ^c and μ^s are the chemical potentials of polymers in crystals and in solutions, respectively. We assume that $\mu^c = 0$ by omitting any disorder defects in the crystals. When the chemical potentials in solid and liquid are equal, we can obtain the equation

$$\begin{aligned}(1-r)\frac{n_2 r}{n} + \ln\frac{qn}{2n_2} + (r-2)\ln\left[1+(q-2)\exp\left(-\frac{E_c}{k_B T_m}\right)\right] \\ = \frac{(r-1)(q-2)}{2}\left[1-\frac{2(r-1)n_2(n+n_1)}{qn^2}\right]\frac{E_p}{k_B T_m} + \frac{r n_1^2}{n^2}\frac{(q-2)B}{k_B T_m}\end{aligned} \tag{4.19}$$

The equilibrium melting point of polymers can be calculated by taking into account all the parameters and solving (4.19).

Figure 4.9 compares the melting temperatures of bulk polymers with different chain lengths derived from the lattice theory, the Flory–Vrij equation and Monte Carlo simulations, respectively. The dimension of the temperature unit is reduced as $E_c/(k_B T_m)$. Although they hold various assumptions, their agreements are satisfying.

4.2.3.3 Comonomer Contents in Random Copolymers

Real polymers are not structurally uniform along the sequences of the chain, and more or less there exist various kinds of irregularities, such as different chemical compositions, different geometrical connections, or different stereo optical isomers

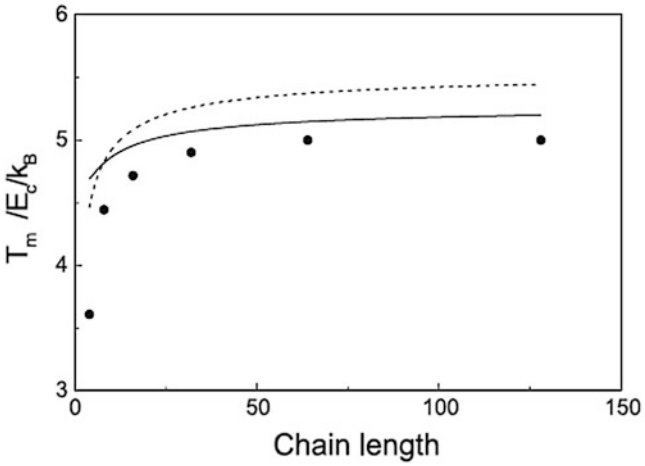

Fig. 4.9 Melting temperature ($T_m/E_c/k_B$) of polymers with different chain length. *The Solid line* is calculated from (4.19) and *dashed line* is results of Flory–Vrij equation. *The Circles* are results from Monte Carlo simulations of polymer solutions with a 0.9375 concentration in a 32^3 cubic lattice for short chains and a 64^3 cubic lattice for long chains (Hu and Frenkel 2005)

of monomers. Because of the spatial mismatch between irregular and regular sequences for the compact packing in crystalline order, the irregular sequences will result in a lowered melting point. If the regular sequences are referred to monomer A and the irregular sequences are referred to comonomer B, Flory (1955) considered this AB random copolymer as an ideal solution and its chemical potential deviation from the sequence-uniform homopolymer A is

$$\mu_{\mathrm{A}}^{\mathrm{co}} - \mu_{\mathrm{A}}^{0} = -RT_{\mathrm{m}} \ln X_{\mathrm{A}} \tag{4.20}$$

Thus, the chemical potential change of crystallization is

$$\mu_{\mathrm{A}}^{\mathrm{c}} - \mu_{\mathrm{A}}^{\mathrm{co}} = \Delta H_{\mathrm{u}} - T_{\mathrm{m}} \Delta S_{\mathrm{u}} \tag{4.21}$$

The subscript "u" represents the unit of mole chain monomers.

For homopolymer composed of monomer A, the chemical potential change of crystallization is

$$\mu_{\mathrm{A}}^{c} - \mu_{\mathrm{A}}^{0} = \Delta H_{\mathrm{u}}^{0} - T_{\mathrm{m}}^{0} \Delta S_{\mathrm{u}}^{0} = 0 \tag{4.22}$$

Considering $\Delta H_{\mathrm{u}}^{0} \approx \Delta H_{\mathrm{u}}$ and $\Delta S_{\mathrm{u}}^{0} \approx \Delta S_{\mathrm{u}}$, the melting point of copolymers can be derived as

$$\frac{1}{T_{\mathrm{m}}} - \frac{1}{T_{\mathrm{m}}^{0}} = \frac{R}{\Delta H_{\mathrm{u}}} \ln X_{\mathrm{A}} \tag{4.23}$$

The similar equation for stereo-optical-isomer copolymers with comonomers homogeneously distributed in the crystallites was also given by Coleman (1958).

Flory assumed all the comonomers staying only in the amorphous phase. By considering comonomers coexisting with monomers in the crystallites, Colson and Eby (1966), and later on Sanchez and Eby (1975) gave another expression for melting point of random copolymers, as given by

$$T_{\mathrm{m}} = T_{\mathrm{m}}^{0} \left(1 - \frac{\Delta H_{\mathrm{B}}}{\Delta H_{\mathrm{u}}} X_{\mathrm{B}} \right) \tag{4.24}$$

In (4.24), ΔH_{B} is the heat of fusion for each comonomer as a defect in the crystalline phase, and X_{B} is the mole fraction of comonomers.

4.2.4 Phase Diagrams of Polymer Solutions

From (4.11), the theoretical curves of L–S coexistence curve and L–L binodal curve can be separately calculated, provided by the absence of each counterpart.

At the equilibrium melting point, the chemical potential of polymers in the amorphous phase μ^s is equal to that in the crystalline phase μ^c, thus

$$\mu^s - \mu^0 = \mu^c - \mu^0 \tag{4.25}$$

where μ^0 is the chemical potential of the ground state where polymer chains are totally extended and packed in parallel with each other. Since in the crystalline phase, μ^c is almost the same as μ^0, we can thus derive that

$$\mu^s - \mu^0 = \frac{\partial \Delta F^s}{\partial n_2} = -kT\frac{\partial \ln Z}{\partial n_2} \approx 0 \tag{4.26}$$

It means

$$\frac{\partial \ln Z}{\partial n_2} = 0 \tag{4.27}$$

Thus, the equilibrium melting point can be calculated by solving the above equation. Changing the polymer concentrations, one can obtain the theoretical phase diagram of L–S coexistence.

The L–L binodal curve can be calculated by the chemical potential equivalence of components between the dense phase and the dilute phase after phase separation. That is,

$$\begin{cases} \Delta\mu_{1a} = \Delta\mu_{1b} \\ \Delta\mu_{2a} = \Delta\mu_{2b} \end{cases} \tag{4.28}$$

where the subscripts "a" and "b" are used to represent the dense and dilute phases, respectively. Before reaching the final result, the mixing free energy as defined as the free energy change of polymer solutions from that of bulk amorphous polymers before mixing should be calculated, as given by

$$\begin{aligned} \frac{\Delta F_{\text{mix}}}{kT} &= \frac{F_{\text{solution}} - F_{\text{bulk}}}{kT} = -(\ln Z - \ln Z_{n_1=0}) \\ &= n_1 \ln \phi_1 + n_2 \ln \phi_2 + n_1 \phi_2 \left[(q-2)\frac{B}{kT} + \left(1 - \frac{2}{q}\right)\left(1 - \frac{1}{r}\right)^2 \frac{E_{\text{P}}}{kT} \right] \end{aligned} \tag{4.29}$$

One can calculate the chemical potentials from (4.29) and insert them into (4.28), the equilibrium concentrations of dense and dilute phases under a certain temperature can be calculated. By changing temperature, the L–L binodal curve is thus obtained.

Monte Carlo simulations can calculate the phase diagrams of polymer solutions in a different way. In the lattice model of polymer solutions, each step of micro-

relaxation in Monte Carlo simulations is determined by Metropolis sampling method with a potential energy barrier as described as

$$\frac{\Delta E}{kT} = \frac{cE_c + pE_p + bB}{kT} = \left(c + p\frac{E_p}{E_c} + b\frac{B}{E_c}\right) / \frac{kT}{E_c} \tag{4.30}$$

where c, p, and b are the numbers of net changes in noncollinear connection, nonparallel packing and mixing pairs of polymer unit and solvent after and before each step, respectively. Figure 4.10 shows the parallel results of liquid–liquid demixing curves and liquid–solid coexistence curves in polymer solutions with different energy parameter sets, obtained from the lattice mean-field theory and Monte Carlo simulations. Theoretical calculations and Monte Carlo simulations agree well with each other, again validating the mean-field theory.

In Fig. 4.10, one can clearly see that the L–S curve is mainly determined by E_p/E_c, and the L–L curve is mainly controlled by B/E_c but is also slightly affected by E_p/E_c. By changing the values of E_p/E_c and B/E_c, the interplay between crystallization and liquid–liquid demixing can be studied in a combination of the lattice theory and parallel molecular simulations (Hu and Frenkel 2004; Ma et al. 2007, 2008), which has been introduced in the author's book (Hu 2013).

In the practical processing of polymers, many organic small molecules such as plasticizers, anti-UV agents and releasing agents are added as diluents, which also result in a depression of melting points. As deduced from Flory–Huggins equation, the chemical potential change in polymer solution is

$$\mu_2^L - \mu_2^0 = RT_m\left[\ln\phi_2 - (r-1)\phi_1 + r\chi\phi_1^2\right] \approx rRT_m\left(-\phi_1 + \chi\phi_1^2\right) \tag{4.31}$$

The chemical potential change upon melting is

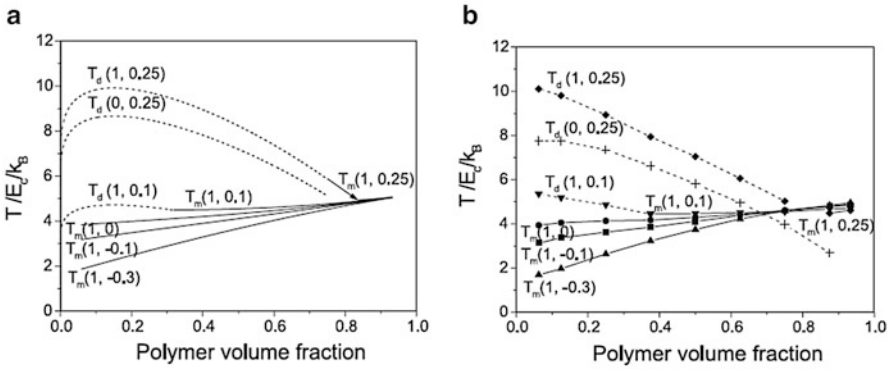

Fig. 4.10 Theoretical calculation (**a**) and Monte Carlo simulations (**b**) of liquid–liquid demixing curves (*dashed lines*) and liquid–solid curves (*solid lines*) of polymer solutions with different energy parameter combinations, denoted by T (E_p/E_c, B/E_c) (Hu et al. 2003a)

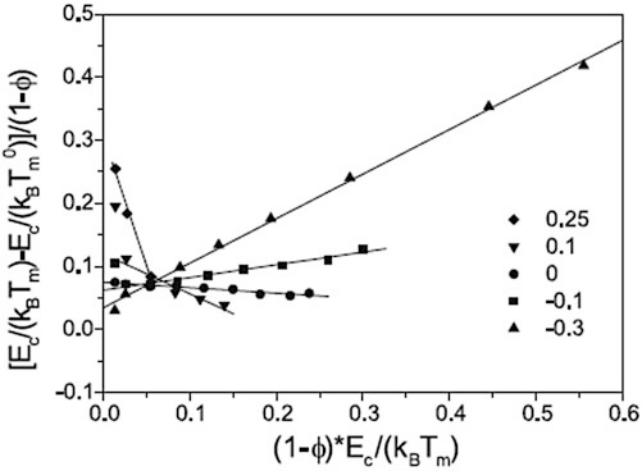

Fig. 4.11 Rescaled data from Fig. 4.10b according to (4.33). The bulk equilibrium melting temperature ($E_c/k_B T_m^0$) is chosen to be approximately 0.2. *Lines* are linear regressions of symbols at the same values of B/E_c as labeled (Hu et al. 2003a)

$$\mu_2^s - \mu_2^0 \approx r\Delta H_u \left(1 - \frac{T_m}{T_m^0}\right) \tag{4.32}$$

ΔH_u is the melting enthalpy of polymers per mole of monomers. When the amorphous phase and the crystalline phase become in equilibrium, their chemical potentials are equal. By combining (4.31) with (4.32) and making them equal to each other, the melting point of polymers in solution is derived as

$$\frac{1}{T_m} - \frac{1}{T_m^0} = \frac{R}{\Delta H_u}\left(\phi_1 - \chi\phi_1^2\right) \tag{4.33}$$

This equation was fitting well with experimental results (Prasad and Mandelkern 1989). It was also verified by the results of Monte Carlo simulations (Hu et al. 2003a). Figure 4.11 shows the linear relationship according to (4.33), with the data points adopted from Fig. 4.10b.

4.3 Kinetics of Polymer Crystallization

4.3.1 Crystal Nucleation

Polymer crystallization can be roughly divided into two sequential processes: crystal nucleation and crystal growth. When the sizes of ordered domains generated by thermal fluctuations become so large that the trend to increase the surface free

energy can be overcome by the trend to decrease the body free energy, larger domains intend to be more stable (Kelton 1991). The critical sizes and the related free energy barriers depend on the crystallization temperature. Therefore, a certain supercooling is required for crystal nucleation. Considering nucleus as a sphere with a radius r, the free energy change of nucleation can be estimated as

$$\Delta G = -\Delta g \times \frac{4}{3}\pi r^3 + \sigma \times 4\pi r^2 \tag{4.34}$$

Δg is the melting free energy of unit volume, and σ is the specific surface free energy. Schematic plot for the free energy change with the increasing radius of nucleus is shown in Fig. 4.12,

Δg in (4.34) is calculated as

$$\Delta g = \Delta h - T_c \Delta s \approx \Delta h - T_c \frac{\Delta h}{T_m} = \Delta h \frac{T_m - T_c}{T_m} \propto \Delta T \tag{4.35}$$

Generally speaking, there are three different types of nucleation according to various dimensions, i.e., primary nucleation, secondary nucleation, and tertiary nucleation. Primary nucleation is a nucleus newly formed by thermal fluctuations, with six extra nucleus surfaces if the nucleus is considered to be cubic. Secondary nucleation is two-dimensional nucleation on the advancing surface of nucleus, with four extra surfaces produced. Secondary nucleation is easier than primary nucleation as its free energy barrier is lower. Tertiary nucleation is one-dimensional nucleation at the step edge of the spreading layer on the advancing surface of nucleus, with only two extra surfaces produced. Tertiary nucleation is so fast that it can rarely be observed. The schematic pictures of different types of nucleation are shown in Fig. 4.13.

Primary nucleation is the most observable phenomenon for the initiation of polymer crystallization, which can be categorized further into homogeneous nucleation and heterogeneous nucleation. In homogeneous nucleation, polymer nuclei can be treated as a cylindrical bunch of stems due to the anisotropic molecular structure, as depicted in Fig. 4.14.

Thus its free energy change during nucleation is

$$\Delta G = -\pi r^2 l \Delta g + 2\pi r l \sigma + 2\pi r^2 \sigma_e \tag{4.36}$$

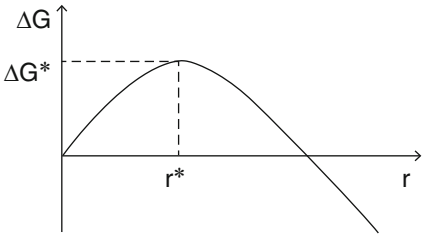

Fig. 4.12 Schematic curve of the free energy change as the radius of nucleus formed in the amorphous phase

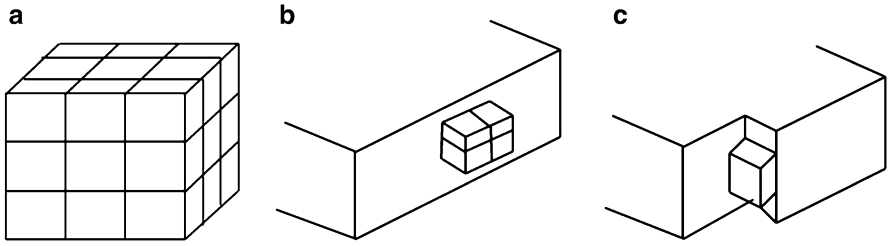

Fig. 4.13 Schematic pictures of (**a**) primary nucleation, (**b**) secondary nucleation, and (**c**) tertiary nucleation

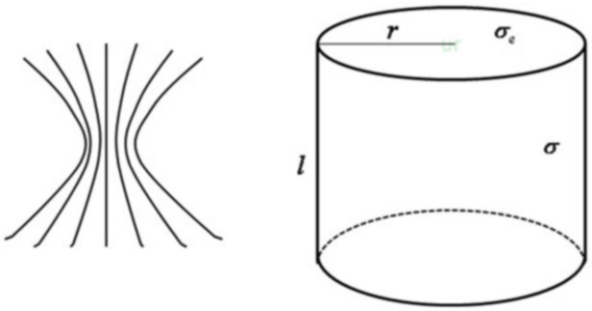

Fig. 4.14 Schematic picture of nucleus treated as cylindrical bunch of stems

Here, r and l are the radius and the length of the cylinder, respectively; σ is the specific free energy on the lateral surface, and σ_e is the specific free energy on the end surface.

By taking the minimum of ΔG with respect to r and l, the critical free energy barrier for nucleation is derived as

$$\Delta G^* = \frac{8\pi\sigma^2\sigma_e}{\Delta g^2} \propto \Delta T^{-2} \tag{4.37}$$

The critical sizes are separately calculated as

$$r^* = \frac{2\sigma}{\Delta g} \propto \Delta T^{-1} \tag{4.38}$$

$$l^* = \frac{4\sigma_e}{\Delta g} \propto \Delta T^{-1} \tag{4.39}$$

So the length-to-radius ratio of the critical nucleus is

$$\frac{l^*}{r^*} = \frac{2\sigma_e}{\sigma} \tag{4.40}$$

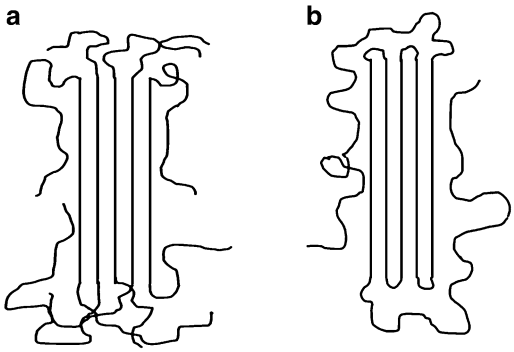

Fig. 4.15 Schematic pictures of (**a**) intermolecular nucleation and (**b**) intramolecular nucleation

For polymers, homogeneous nucleation can be realized through two typical ways. One is the so-called *intramolecular nucleation* (Wunderlich 1976) featured with adjacent chain-folding, which can be called as chain-folding nucleation. The other is the so-called *intermolecular nucleation* composed of parallel stacking among neighboring chains, which can be called as fringed-micelle nucleation. Schematic illustration of these two models can be found in Fig. 4.15.

Let us first consider the intramolecular nucleation. The specific free energy on the lateral surfaces of PE crystals was estimated to be 11.8 erg/cm^2, and its specific free energy on the fold-end surface was about 90 erg/cm^2 (Hoffman and Miller 1997). By (4.40), the optimized aspect ratio of critical nucleus is 15.3. Now look at the intermolecular nucleation. The end surface has an extra free energy of about 245 erg/cm^2 as estimated by Zachmann (1967, 1969), due to the entropy loss of disordered chains. So the aspect ratio of critical nucleus in intermolecular nucleation is as high as 56.8, and it appears very difficult to produce such kind of fibril nucleus through thermal fluctuations for primary nucleation. Moreover, by (4.36), the higher end-surface free energy results in a higher nucleation barrier than the chain-folding model. So from both kinetics aspects of the critical nucleation barrier and of thermal fluctuations, the intramolecular nucleation is preferred in the process of primary nucleation.

Heterogeneous nucleation is primary crystal nucleation on the foreign surfaces of other materials such as catalysts, dusts, and container walls. Because less extra surface free energy is required, heterogeneous nucleation is much easier than homogeneous nucleation. Assuming that heterogeneous nucleus is a cubic nucleus, its free energy barrier is similar like homogeneous nucleation, again depending upon inverse square supercooling. When the foreign surface free energy is close to that of polymer crystals, the heterogeneous nucleation is more like a layer-by-layer growth on the foreign surface. We assume that a, b_0, and l are its width, depth, and length, respectively, as shown in Fig. 4.16, the free energy change of nucleation is given by

$$\Delta G = -ab_0 l\Delta g + 2b_0 l\sigma + al\Delta\sigma + 2ab_0\sigma_e \tag{4.41}$$

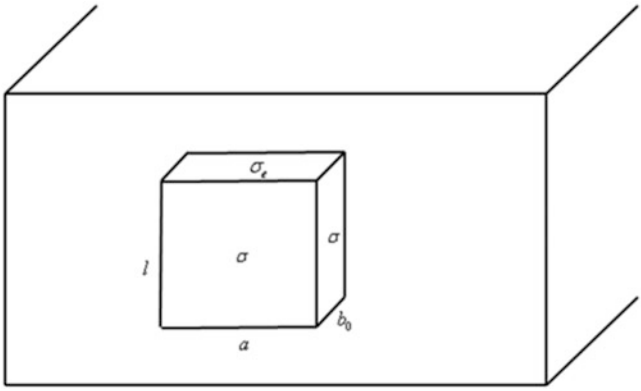

Fig. 4.16 Schematic picture of heterogeneous nucleation

In (4.41),

$$\Delta\sigma = \sigma + \sigma_{cs} - \sigma_{ms} \tag{4.42}$$

σ_{cs} is the surface free energy between crystal nucleus and substrate, and σ_{ms} is the surface free energy between melt and substrate. If the free energy of substrate is almost the same as crystal nucleus, $\Delta\sigma \approx 0$, by minimizing ΔG of a and l separately, the critical Gibbs free energy is

$$\Delta G^* = \frac{4b_0\sigma\sigma_e}{\Delta g} \propto \Delta T^{-1} \tag{4.43}$$

There is also another type of primary nucleation called self-nucleation investigated first by Blundell et al. (1966). The foreign surfaces for self-nucleation are provided by crystals of the same species which survived during thermal history. Since there is no extra surface free energy change during self-nucleation, it is also called athermal nucleation. This type of nucleation is an important source of memory effects for polymer crystallization.

The nucleation rate is dominated by two factors. One is the critical free energy barrier of nucleation. Its exponential dependence was first proposed by Volmer and Weber (1926). The other is the diffusion energy barrier for molecules crossing over the liquid–solid interfaces. Its exponential dependence was first proposed by Becker and Döring (1935). The quantitative expression of the prefactor in the kinetic equation of the nucleation rate is given by Turnbull and Fisher (1949) as

$$I = I_0 \exp\left(-\frac{\Delta E + \Delta G^*}{kT}\right) \tag{4.44}$$

where ΔE is the activation barrier for short-range diffusion over the liquid–solid boundary, and I_0 is the prefactor. The critical free energy barrier is proportional to

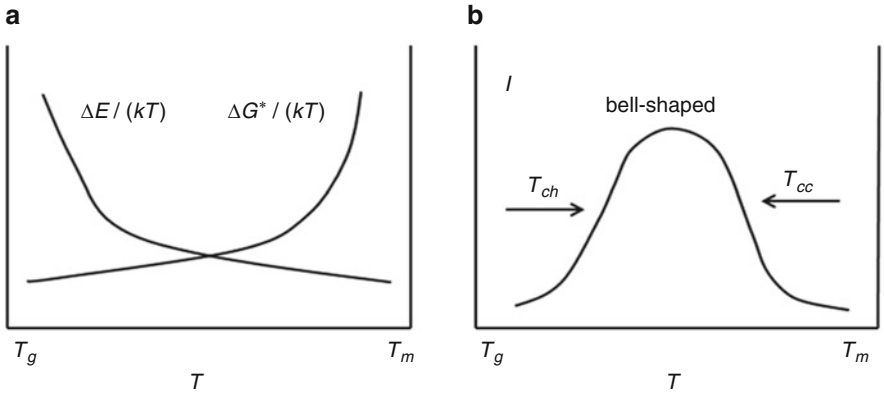

Fig. 4.17 Schematic illustration on the temperature dependence (**a**) of the critical free energy barrier and the activation barrier for diffusion, and (**b**) of the bell-shape curve of the nucleation rates

the inverse square supercooling of primary nucleation. So when temperature is high with a high free energy barrier, the nucleation rate is small. However, when temperature is low with a high activation barrier for polymer diffusion, the nucleation rate is again small. Thus, the temperature-dependence curve of the nucleation rate is somewhat like a bell shape between the glass transition temperature and the melting temperature, as illustrated in Fig. 4.17.

At high temperatures, the kinetic studies of polymer crystallization is mostly focused on the nucleation. In this region, heterogeneous nucleation takes place and the resulted mechanical properties of the semicrystalline polymers are usually hard and brittle. While in the region of low temperatures, as a result of high density of small crystallites, the semicrystalline polymers become soft and tough.

Intramolecular nucleation is preferred in polymer crystal nucleation, both primary and secondary. The secondary intramolecular nucleation explains why chain-folding is a kinetic preference, which results in lamellar shapes during crystal growth. The typical intramolecular nucleation was investigated by Monte Carlo simulations of crystal nucleation of a single-chain system (Hu et al. 2003b). Taking the extended single chain in a crystal composed of extended parallel polymer chains as the ground state, and assuming the number of melting bonds n, the free energy change of the chain is

$$\Delta F = \Delta f n + \sigma(N-n)^{2/3} \tag{4.45}$$

where Δfn is the bulk free energy change and $\sigma(N-n)^{2/3}$ is the surface free energy change. The free energy change of one bond during melting is

$$\Delta f = \frac{q-2}{2} E_{\mathrm{p}} - kT\ln(q-1) \tag{4.46}$$

The first term on the right-hand side means $q-2$ parallel bonds around the bond in the ground state, and the denominator "2" is the symmetric factor. The number of total conformation of a chain with n melting bonds is $(q-1)^n$, so the second term is the average conformational entropy change of each bond during melting.

When the system is in equilibrium, the free energy in the disordered state is equal to that in the ordered state, then

$$\Delta f_e = \sigma N^{-1/3} \tag{4.47}$$

And the equilibrium free energy barrier for primary nucleation is (Fig. 4.18)

$$\Delta F_e = \frac{4\sigma^3}{27\Delta f_e^2} \tag{4.48}$$

The free energy barriers for crystallization and melting of a single chain are separately calculated as follows,

$$\Delta F_c = \frac{4\sigma^3}{27\Delta f^2} \tag{4.49}$$

$$\Delta F_m = \frac{4\sigma^3}{27\Delta f^2} + \Delta f N - \sigma N^{2/3} \tag{4.50}$$

Equations (4.49) and (4.50) are confirmed by Monte Carlo simulations, as shown in Fig. 4.19. Single chains with different lengths will crystallize at the same temperature on cooling, but will melt at different temperatures on heating, with higher melting temperatures for higher chain lengths. In bulk polymers, the nucleation rates appear chain-length dependent, probably because the prefactor in the kinetic equation of nucleation could also be of chain-length dependence.

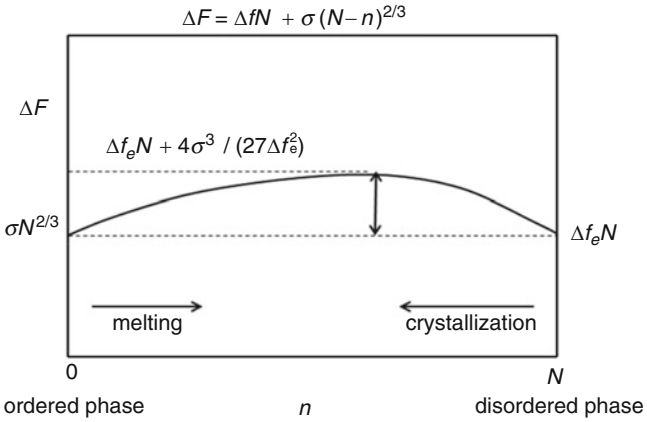

Fig. 4.18 Schematic free energy of single chain with number of melting bonds under thermal equilibrium state (Hu et al. 2003b)

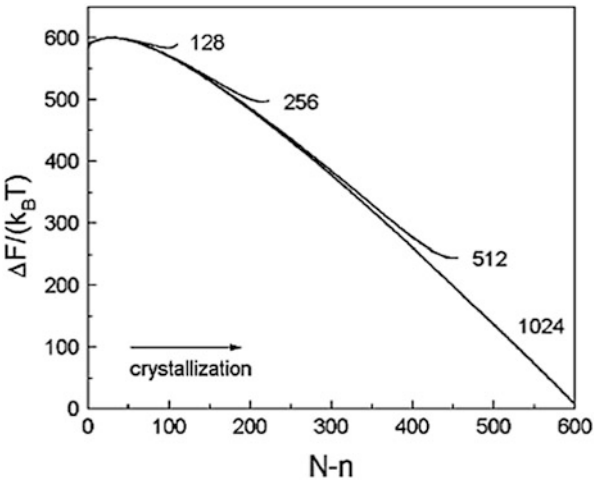

Fig. 4.19 Free energy curves with various crystalline bonds at the fixed temperature $T = 2.174\,E_p/k_B$ in the single chain systems with different chain lengths as labeled (Hu et al. 2003b)

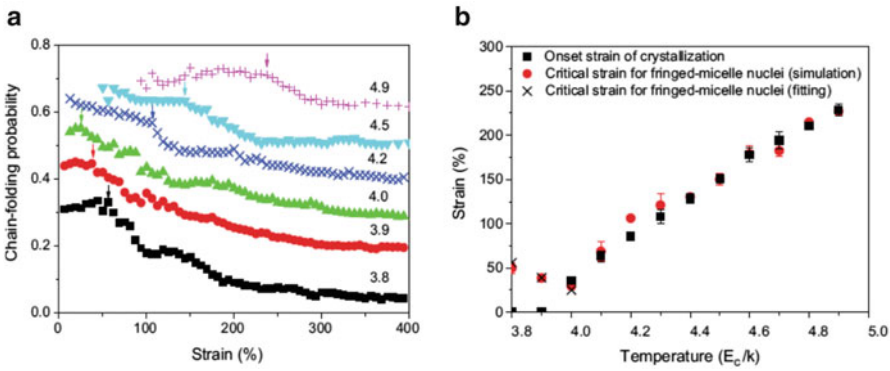

Fig. 4.20 (**a**) Strain-evolution curves of chain-folding probability of small crystalline clusters containing 50–200 parallel packed bonds under different temperatures. The *lines* are vertically shifted by 0, 0.15, 0.25, 0.35, 0.45, and 0.55, respectively. (**b**) Comparison between the onset strains of crystallization and the critical strain for fringed-micelle nuclei under different temperatures (Nie et al. 2013)

It should be noted that intermolecular nucleation could coexist with intramolecular nucleation. Intermolecular nucleation is often observed with short chains, rigid chains, polymerizing chains, or when chains are stretched. Recently, upon stretching network polymers, the transition from intramolecular nucleation to intermolecular nucleation was observed in Monte Carlo simulations (Nie et al. 2013). By analyzing the probability of adjacent chain-folding of those newly formed crystallites with a size between 50 to 200 parallel packed bonds at each step of stretching, an obvious reduction was observed in its evolution curve under each temperature as shown in Fig. 4.20a. The corresponding critical strain was considered to be the transition point under which intramolecular nucleation is the favorite and above which intermolecular nucleation becomes the dominant.

Compared the critical strain with the onset strain of crystallization during stretching under each temperature as shown in Fig. 4.20b, it is found that at low temperatures (the dimension-reduced $T \leq 4.0$) intramolecular nucleation dominates the initiation of polymer crystallization with a smaller strain than the critical value, and when temperature becomes higher, intermolecular nucleation begins to dominate the initiation of crystallization.

Recently, some researchers proposed a preordered structure in the polymer melt before nucleation. Imai and coworkers attributed the preordered structures to spinodal decomposition during orientational fluctuations at low temperatures for cold crystallization of PET (Imai et al. 1993, 1994). The main proof came from the observation of small-angle X-ray scattering (SAXS) signal before wide-angle X-ray diffraction (WAXD) during isothermal crystallization at low temperatures (Terrill et al. 1998). Sirota and Herhold (1999) and Kraack et al. (2000) observed a mesophase of chain cluster at the early stage of nucleation of long alkane chains and there is almost no supercooling for nucleation although the mesophase disappears as soon as chain-folding occurs in the crystallization of long-enough chains (Sirota 2000). The idea of nucleation initiated by spinodal decomposition was then prevailing in many theoretical models. Olmsted and coworkers (1998) thought spinodal decomposition is a result of coupling between orientational-order fluctuations and density fluctuations at low temperatures. The spinodal decomposition will enhance crystal nucleation at a certain supercooling. In molecular dynamics simulations, Gee and coworkers (2005) observed that the crystallization behaviors of PVDF under 600 K and PE under 450 K in a time scale of nanoseconds appear as spinodal decomposition. Milner calculated the free energy change of PE crystal nucleation through a rotated mesophase, and it is lower than the surface free energy of orthogonal crystalline phase. He thought this could be the free energy barrier for crystal nucleation (Milner 2011). However, the prior occurrence of SAXS signal could be attributed to a limited instrument sensitivity or improper experiment treatment. Howard Wang thought that the signal like that of spinodal decomposition could be expected as a result of improper over-reduction in the empty correction (Wang 2006). Wang et al. (2000) attributed the phenomenon to instrument sensitivity of WAXD for the small number of crystallites in the early stage of crystallization. Indeed, improving the sensitivity of WAXD by four magnitudes, the difference between SAXS and WAXD disappeared at low temperatures as observed by Heeley et al. (2003). The remained difference at high temperatures can be associated to heterogeneous nucleation rather than homogeneous nucleation.

4.3.2 Crystal Growth

4.3.2.1 Secondary Nucleation Models

After primary crystal nucleation, crystals begin to grow. The crystal growth may be diffusion-controlled or interface-controlled. If crystal grows under a large supercooling in dilute polymer solutions, the growth rate is mainly controlled by

a long-distance diffusion from the far-away bulk solution to the crystal surface. This is referred to the diffusion-controlled mechanism. The linear crystal growth rate is

$$v = \frac{\mathrm{d}r}{\mathrm{d}t} \propto t^{-1/2} \tag{4.51}$$

The diffusion-controlled mechanism means that the crystal size is not linearly dependent on the growth time (Holland and Lindenmeyer 1962). In the commonly practical cases, crystal growth is controlled by the process at the advancing surface of the crystal. This is referred to the interface-controlled mechanism. When controlled by this mechanism, the linear crystal growth rate is independent of time. The interface-controlled mechanism can be further separated into three categories, i.e., secondary nucleation growth, screw dislocation growth, and surface roughing growth. The secondary nucleation is prevailing in the description of the kinetics of lamellar polymer crystal growth (Flory and McIntyre 1955; Burnett and Mcdevit 1957; Wunderlich and Cormier 1966; Wunderlich et al. 1967).

In experiments, for example, by small-angle laser scattering (SALS) on small crystallites, or by polarized light microscope (PLM) on large crystallites, it is found that the growth rate of lamellar crystals is independent of time. This behavior implies the surface-controlled mechanism for crystal growth. Thickening at the growth front is also observed in many experiments (Wunderlich and Mielillo 1968; Abo El Maaty and Bassett 2005; Mullin and Hobbs 2011). So the crystal growth process can be treated as two steps at the wedge-shaped growth front, secondary nucleation occurs first, followed with instant thickening until thickness becomes larger than the minimum thickness for further growth of lamellar crystals. Secondary nucleation dominates the temperature dependence of the growth rate, and thickening provides the driving force for crystal growth. As will be introduced below, Lauritzen-Hoffman model and its developments dominated the present understanding of growth kinetics of lamellar crystals. The intramolecular nucleation model recently provided a promising progress.

The linear crystal growth rate of lamella by lateral-surface advancing can be treated as the competition result between advancing rate and melting rate of the growth front. Taking intramolecular secondary nucleation as the rate-determining steps for both crystal growth and melting, they need to overcome the same nucleation energy barriers from mutually opposite directions. It is the difference of the two energy barriers ΔG that determines the linear growth rate, as derived according to (4.44) by

$$\begin{aligned} v &= v_{\text{growth}} - v_{\text{melting}} = v_{\text{growth}}\left(1 - \frac{v_{\text{melting}}}{v_{\text{growth}}}\right) \\ &= v_{\text{growth}}\left(1 - \exp\left(-\frac{\Delta G}{kT_c}\right)\right) \end{aligned} \tag{4.52}$$

Assuming ΔG is very small as reflected by the excess lamellar thickness above the minimum, and replacing the exponential term by the first two terms of Maclaurin expansion $(\exp(x) = 1 + x + x^2/2 + x^3/6 + \cdots + x^i/i! + \cdots)$, we can get the linear growth rate as

$$v \approx v_{\text{growth}} \frac{\Delta G}{kT_c} = v_{\text{growth}} (l - l_{\min}) \frac{b^2 \Delta g}{kT_c} \tag{4.53}$$

In (4.53), the term $l - l_{\min}$ determines the net free energy for crystal growth, b is the average distance between stems inside the crystal, and Δg is the free energy change for melting of unit volume. Thus, we can treat v_{growth} in (4.53) as the free energy barrier for crystal growth and the rest part as the driving force for crystal growth (Ren et al. 2010). Under low temperatures, $l > l_{\min}$ and the crystal will grow, while under high temperatures, $l < l_{\min}$ and the crystal will melt. So temperature variation can lead to a continuous switching between growth and melting at the lateral growth front of lamellar crystals (Ren et al. 2010).

Lauritzen–Hoffman (LH) theory is still the most widely used theoretical model in the explanation of the growth kinetics of lamellar crystals. Figure 4.21 schematically shows the basic assumptions of folded stems at the growth front in the LH theory, without considering the thickening at the lateral growth front.

The LH theory holds four basic assumptions as listed below.

1. The growth front of polymer crystal is smooth. Secondary nucleation begins with a first stem deposited at the growth front, and follows with lateral spreading until reaching the lateral edges of the front substrate.
2. The chain-folded length l is constant during crystal growth. The width, thickness and number of stems are separately a_0, b_0 and v.
3. The number of growth fronts holding v stems N_v is in a steady-state distribution.
4. Each stem should go through an activation state before entering the crystal lattice where the fraction in each stem successfully entering the crystal lattice is ϕ.

If the number of grown stems is v, the change of Gibbs free energy is

$$\Delta G = 2b_0 l\sigma + 2(\nu - 1)a_0 b_0 \sigma_e - \nu a_0 b_0 l \Delta g \tag{4.54}$$

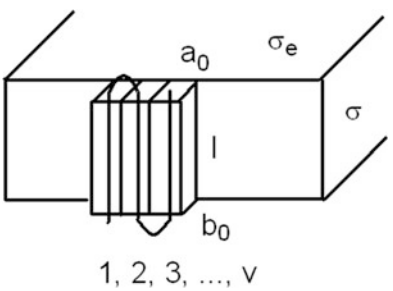

Fig. 4.21 Schematic picture of folded stems at the growth front considered in the LH theory

When $v = 1$, the growth rate for the first stem is

$$A_0 = \beta \exp\left(-\frac{2b_0 l\sigma - \phi a_0 b_0 l\Delta g}{kT}\right) \tag{4.55}$$

The melting rate of the first stem is

$$B_0 = \beta \exp\left(-\frac{(1-\phi) a_0 b_0 l\Delta g}{kT}\right) \tag{4.56}$$

If $v > 1$, the growth rate of the rest stems is

$$A = \beta \exp\left(-\frac{2a_0 b_0 \sigma_e - \phi a_0 b_0 l\Delta g}{kT}\right) \tag{4.57}$$

The melting rate of the rest stems is

$$B = B_0 \tag{4.58}$$

where β is a kinetic prefactor defined as

$$\beta = \frac{kT}{h} \exp\left(-\frac{\Delta E}{kT}\right) \tag{4.59}$$

By the assumption of a stable distribution of the growth fronts in the steady state, the growth flux of fronts is

$$S = N_0 \beta \exp\left[-(2b_0\sigma - \phi a_0 b_0 \Delta g_f)\frac{l}{kT}\right]\left[1 - \exp\left(\frac{2a_0 b_0 \sigma_e - a_0 b_0 l\Delta g_f}{kT}\right)\right] \tag{4.60}$$

Different growth crystals contain different folded lengths. $S(l)$ is the crystal growth flux with folded length l. Thus, the average length of all the crystals is calculated as

$$\langle l \rangle = \frac{\int_{l_{min}}^{\infty} lS(l)\mathrm{d}l}{\int_{l_{min}}^{\infty} S(l)\mathrm{d}l} \tag{4.61}$$

The result of (4.61) is

$$\langle l \rangle = \frac{2\sigma_e}{\Delta g} + \frac{kT}{2b_0\sigma} \times \frac{2 + (1-2\phi)a_0\Delta g/(2\sigma)}{[1 - \phi a_0 \Delta g/(2\sigma)][1 + (1-\phi)a_0\Delta g/(2\sigma)]} \tag{4.62}$$

where $2\sigma_e/\Delta g$ is the minimum length for steady growth. Equation (4.62) is used to predict the average thickness of lamellar crystals grown at different temperatures.

Besides an explanation of chain-folding lengths, the phenomenon of regime transitions can also be explained by the LH theory. If crystal growth is controlled by secondary nucleation, the temperature dependence of crystal growth rates can be dominated by

$$G = G_0 \exp\left(-\frac{U}{T - T_0}\right) \exp\left(-\frac{K_g}{T\Delta T}\right) \tag{4.63}$$

The first exponential term is attributed to short-range diffusion across the interface and the second term is attributed to secondary nucleation with the nucleation barrier proportional to the inverse supercooling. When temperature is high enough, crystal growth rate becomes mainly controlled by secondary nucleation. In this case, the curve of $lgG + U/(T - T_0)$ versus $-1/T/\Delta T$ can be divided into three linear regimes with the lowering of temperature, and the ratios of K_g among three regimes are

$$K_g(\mathrm{I}) : K_g(\mathrm{II}) : K_g(\mathrm{III}) = 2 : 1 : 2 \tag{4.64}$$

The above ratio is the so-called regime-transition phenomenon, which can be explained on the basis of secondary nucleation assumed in the LH theory. When crystallization takes place at a very high temperature, the rate of secondary nucleation i becomes the rate-determining step, and the followed surface spreading rate g is very large, so $i < g$. The secondary nucleation is supposed under the determination of the free energy barrier for depositing the first stem (Lauritzen and Hoffman 1960; Hoffman and Lauritzen 1961; Hoffman et al. 1976). Once the nucleus becomes stable, it will spread to the two lateral sides very fast with a layer thickness of b. The growth front with the width L is smooth until the next nucleus shows up. This temperature range is referred to Regime I and the crystal growth rate in this regime is

$$G_{\mathrm{I}} = ibL \tag{4.65}$$

Molecular simulations have reproduced regime-transition phenomena (Hu and Cai 2008). However, the growth front of Regime I is rather rough, favoring an alternative interpretation based on the intramolecular secondary nucleation model (Hu and Cai 2008).

When temperature is lower than Regime I, the rate of secondary nucleation becomes higher and $i \sim g$. Several nuclei will grow together and the growth front will no longer be smooth. This temperature range is referred to Regime II. The advancing rate is proportional to the square root of secondary nucleation rate i, as given by

$$G_{\mathrm{II}} = b(2gi)^{1/2} \tag{4.66}$$

If the temperature is further lower than Regime II, secondary nucleation rate becomes much larger than the spreading rate, $i > g$. In this case, several crystal

layers will grow at the same time, each layer with several nuclei and the distance between two nuclei is L'. This temperature range is referred to Regime III and the crystal growth rate is

$$G_{\mathrm{III}} = ibL' \tag{4.67}$$

In the LH theory, chain-folded length was assumed to be constant and thickening was omitted during crystal growth. Also the free energy barrier for secondary nucleation was assumed to be determined by the first stem, and no more stem was considered. These assumptions are not so reasonable and many other models (Armistead and Goldbeck-Wood 1992) have been proposed in order to reach a better understanding about the growth kinetics of lamellar crystals.

Wunderlich and Arakawa observed the layer structure of PE crystal under atmospheric pressures higher than 3 kbar and the crystallinity was almost 100 % (Prime and Wunderlich 1969). In the crystals, polymer chains were perpendicular to the lamella and the largest thickness was even larger than the molecular length, which indicated the existence of extended chains in the crystals (Olley and Bassett 1977). By further observation of the lamella growth front, Wunderlich found the wedge-shaped growth front and proposed a thickening-growth mechanism under high pressures (Wunderlich 1976). In his explanation, molecular nucleation or secondary nucleation firstly took place at the growth front, and later-on developed into extended-chain crystals by fast thickening. By observing the growth process of PE folded-chain crystal (FCC) and extended-chain crystal (ECC), Hikosaka developed the growth mechanism with chain-sliding diffusion for thickening, on the basis of the LH theory (Hikosaka 1987, 1990). In his equation of nucleation rate, the free energy barrier for short-range diffusion across the interface was also considered besides the free energy barrier of critical nucleus. The growth appears as two-dimensional, which holds both lateral and longitudinal growth of the chain stems. The two-dimensional nucleation growth mechanism can be used to explain the dependence of lamella thickness on supercooling near the triple point of high pressures (Hikosaka et al. 1995).

Wunderlich and Mehta put forward the concept of molecular nucleation (Wunderlich and Mehta 1974; Mehta and Wunderlich 1975; Wunderlich 1979; Cheng and Wunderlich 1986) in order to explain the molecular weight effect in crystallization of PE and some other polymers. At very high temperatures, the fraction of high molecular weights will crystallize first. It was proposed that each molecule entered the crystal with an additional nucleation barrier. Chain-folded secondary nucleus formed by molecules with enough lengths can only be stabilized over the critical size, while short-chain nucleus will be melted again, as illustrated in Fig. 4.22. The concept of molecular nucleation can be regarded as a patch on the LH model.

The free energy change of molecular nucleation at the growth front is

$$\Delta G = -abl\Delta g + 2bl\sigma + 2(n-1)ab\sigma_{\mathrm{e}} + 2ab\sigma_{\mathrm{e}}' \tag{4.68}$$

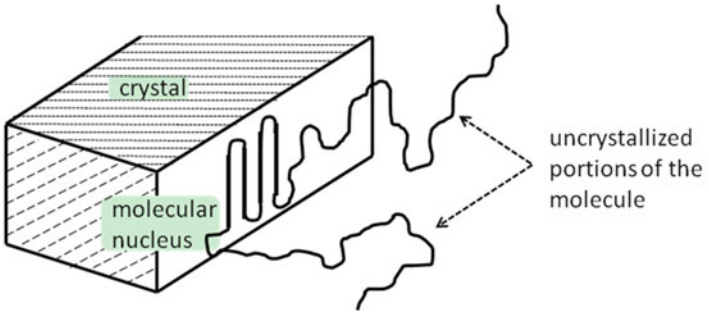

Fig. 4.22 Schematic picture of molecular nucleation (Wunderlich 2005)

σ_e is the surface free energy with chain cilia, thus the free energy change of critical nucleus is

$$\Delta G^* = \frac{4b\sigma\sigma_e}{\Delta g} + 2ab\sigma_e' \tag{4.69}$$

This critical free energy barrier is higher than normal secondary nucleation and thus the molecular nucleation can be the rate-determining step of crystal growth.

The intramolecular nucleation was then developed by supposing that all the secondary nucleation is mainly controlled by intramolecular nucleation (Hu et al. 2003b; Hu 2007) and the basic crystal lamella is resulted due to the preference of chain-folding in this unique style of secondary nucleation.

Assuming secondary nucleation of a single chain at the two-dimensional locally smooth growth front, the free energy change based on the classical nucleation theory is

$$\Delta F = \Delta f n + \sigma(N-n)^{1/2} \tag{4.70}$$

The free energy barrier for crystal nucleation is

$$\Delta F_c = \frac{\sigma^2}{4\Delta f} \tag{4.71}$$

And the equilibrium free energy barrier is

$$\Delta F_e = \frac{\sigma^2}{4\Delta f_e} \tag{4.72}$$

The free energy barrier for critical intramolecular nucleation under a certain temperature is independent of chain length, but not for the opposite direction, i.e., melting. Therefore, a critical molecular length exists for the equilibrium

intramolecular melting at the growth front under each temperature. For a polymer sample with a polydispersity of molecular weights, only the fractions of chain lengths larger than the critical length can be stable and thus enter the crystal during secondary nucleation. This is the reason why molecular segregation occurs upon lamellar crystal growth. Molecular segregation can be observed only in polymer crystallization under very high temperatures.

Under a low temperature, the critical chain length for secondary nucleation may be much smaller than the chain length, and several events of intramolecular nucleation could happen along the same chains. If they occur in the same lamellar crystal, loops are formed; and if in different lamellar crystals, tie molecules are formed. The intramolecular nucleation model allows a statistical treatment on the semicrystalline texture.

The spreading right after the event of intramolecular nucleation may be stopped by the entanglements of long chains, collisions of nuclei at the same growth fronts, or the limited width at the growth front. Monte Carlo simulations (Hu et al. 2003c) have demonstrated that a single chain enters into the crystal growth front via several events of surface nucleation along the chain, as a result of limited growth-front sizes.

Besides molecular segregation (Hu 2005), many other phenomena unique for polymer crystal growth also favor the intramolecular nucleation model, such as co-crystallization of long and short chains (Cai et al. 2008; Jiang et al. 2015) as well as the interpretation of regime transitions (Hu and Cai 2008).

4.3.2.2 Other Non-nucleation Models

There are some models based on non-nucleation mechanisms for lamellar crystal growth. The (200) growth front of PE single crystals will become curvature when crystallization temperatures are very high, which could not be explained by the LH theory based on secondary nucleation growth on smooth surface. Also a pair of concave (110) surfaces were observed in the twin single crystal, which means the free energy barrier from side surfaces may not be the main problem for the advancing of the growth front (Sadler et al. 1986). Based on these observations, Sadler and Gilmer (1988) (SG) proposed the row model of continuous growth along the direction perpendicular to the growth front, as illustrated in Fig. 4.23.

In the SG model, crystal unit will be randomly added in or be removed from the growth front with a free energy change. On the one hand, the longer the growth stem, the larger the driving force for advancing the growth front. The driving force is proportional to the difference between the stem length and the critical length for a stable stem. On the other hand, the thicker the growth front, the longer time needed to reach the critical stem length because chain extending is pinned by the metastable chain-folding or loops. The possibility of stem lengths among all the conformations is only

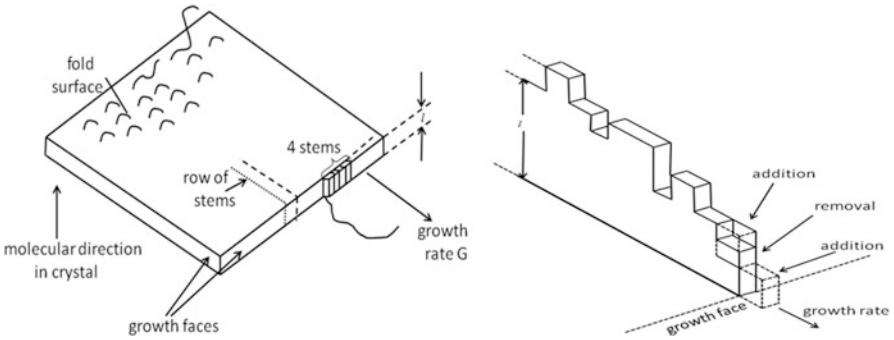

Fig. 4.23 Schematic pictures of the row model proposed by Sadler and Gilmer (1988)

$$P = e^{-kl} \tag{4.73}$$

Thus, the total growth rate is

$$G \propto e^{-kl}(l - l_{\min})\Delta g/(kT) \tag{4.74}$$

The stem lengths exhibit two opposite trends of contributions to the total growth rate, and the maximum of growth rate will be realized at a certain stem length, which explains the growth thickness of the lamellar crystals. The thickness can be calculated as

$$\langle l \rangle = l_{\min} + \frac{1}{k} \tag{4.75}$$

Like in the LH theory, the free energy barrier for crystal growth in the SG model is related directly with the lamellar thickness without considering further thickening after crystal growth. Also, the proposed thermal roughening may still be flat at the crystal edge, without the necessity of curvature at the growth surface.

In both LH and SG models, the growth front was supposed to directly reach the critical thickness in the growth process, and the thickening after growth was neglected, which appears not so reasonable. Keller and coworkers (Keller 1992; Keller et al. 1994) proposed a wedge-shaped growth-front model considering an obvious thickening in the crystal growth process of PE, as illustrated in Fig. 4.24.

In the wedge-shaped growth model, the melt may first grow into a mesophase (hexagonal phase) in the thinnest region of the growth front. The mesophase is stable because of large specific surface energy of small crystallites, which is referred as the finite-size effect. Then, the thin lamella thickens into the stable orthogonal phase, which decides the lamellar thickness. There is a triple point Q, as demonstrated in Fig. 4.25. If temperature is above the triple point temperature, the melt will grow into the orthogonal phase directly. If temperature is below the triple point, there will be mesophase.

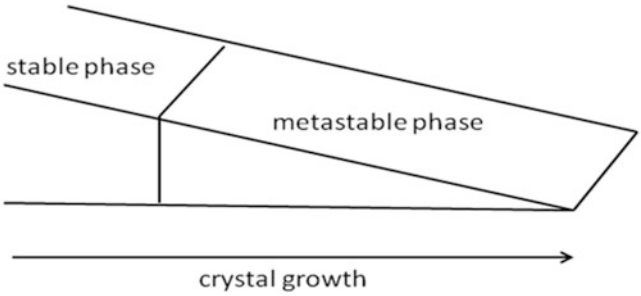

Fig. 4.24 Schematic picture of wedge-shaped growth front of PE lamella

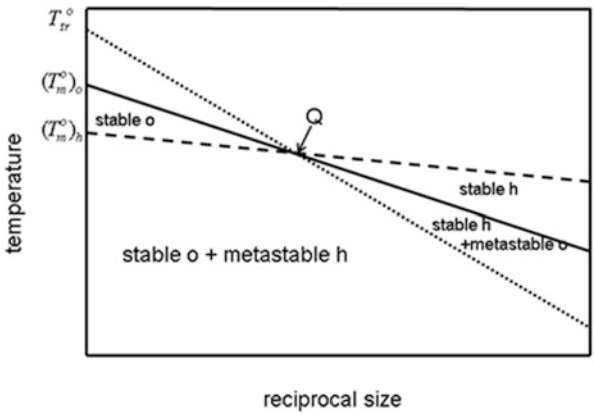

Fig. 4.25 Schematic picture showing temperature against reciprocal thickness of polyethylene crystals

This model was later on expanded by Strobl (2000, 2005, 2006, 2009) to other polymers, in order to explain the experimental observations of his group, as illustrated in Fig. 4.26.

There is a linear relationship between the crystallization temperatures and the inverse lamella thicknesses, which is quite in accordance with Gibbs–Thomson equation. There is also a linear relationship between the melting temperatures and the inverse lamella thicknesses. Crossover of these two linear curves is considered to be the triple point of mesophase transition. Recently, the crossover was reproduced in the molecular simulations of lattice polymers, and the interpretation was updated to an uplimit of instant thickening at the lateral growth front of lamellar crystals (Jiang et al. 2016).

Allegra (Allegra 1977, 1980; Allegra and Meille 1999, 2005) proposed statistical thermodynamic theory for the mesophase of small crystallites or crystal cluster in the metastable disordered phase before crystallization. The cluster will first grow into a stable size and then joins into the crystal, as illustrated in Fig. 4.27. The thickness of lamella is decided by the cluster size. Zhang and Muthukumar (2007) performed simulations of clusters to form single crystals grown in dilute solutions, consistent with the experimental observations.

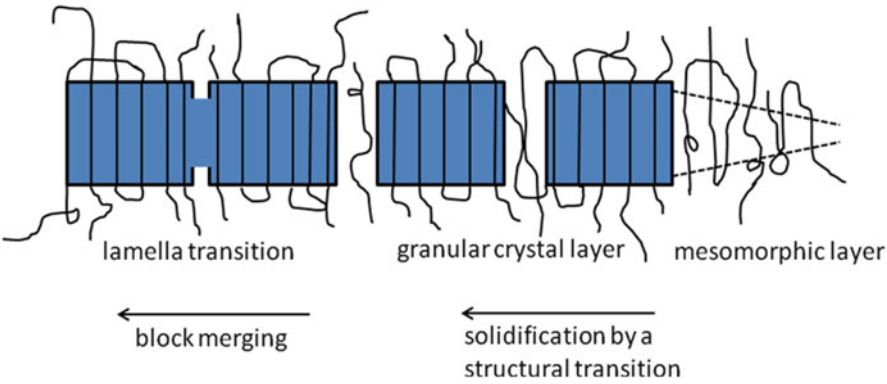

Fig. 4.26 Schematic picture of mesophase at the growth front in lamella (Strobl 2009)

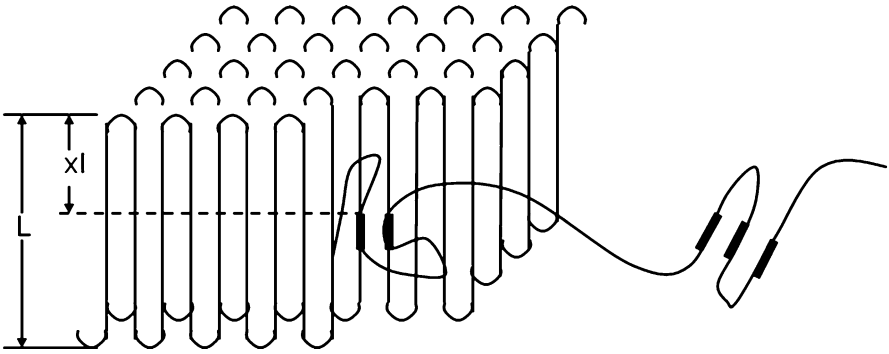

Fig. 4.27 Schematic picture of equilibrium-sized cluster growth model (Allegra and Meille 2005)

Muthukumar and coworkers (Welch and Muthukumar 2001; Muthukumar 2005) gave a thermodynamic explanation to the lamella thickness. He thought that the finite lamella thickness was a result of the largest thermodynamic stability of small crystallites. The crystalline chain will find the folded length related to the minimum free energy of the whole crystallite although there is a free energy barrier for the thickening of integer folding. The mechanism for crystal growth to select a limited lamellar thickness is recently addressed by the combination of secondary nucleation and instant thickening at the lateral growth front of lamellar crystals (Jiang et al. 2016).

4.3.3 Crystal Annealing

Annealing is a procedure to keep the temperature of a crystal body near its melting point so as to relax its inner stress and to remove defects. When annealing is used for polymer materials, it can make metastable polymer crystals more perfect and more stable. If the annealing temperature is low, it just makes the crystal more

perfect by removing defects from crystal lattice. As a result, crystallinity is increased. If the annealing temperature is high, crystal thickening will happen and results in more stable crystals. If the annealing temperature is very high, even higher than the melting point of metastable crystals, crystals may melt and recrystallize into a more stable state unless the temperature is close to the equilibrium melting point of infinitely large crystals.

There are two mechanisms to explain lamellar thickening, one is *solid-chain sliding-diffusion* mechanism, and another is *melting-recrystallizaiton* mechanism. Peterlin (1963) proposed an activation energy barrier for sliding diffusion of folded chains in monolayer crystals, trying to explain why the folded length of polymer chains increases linearly with the logarithm of time. The sliding-diffusion mechanism was then developed into a more general theory by Sanchez and his collaborators (1973, 1974). Dreyfus and Keller (1970) proposed the fold-dislocation thickening model, in which the lamellar thickness can be doubly increased, as schematically demonstrated in Fig. 4.28. Another is the melting-recrystallization mechanism, which was firstly reviewed by Fischer (1969) and then introduced by Wunderlich (1976) in his famous book. This mechanism was confirmed by several experimental phenomena, such as decrease-then-increase of crystallinity in the annealing process (Matsuoka 1962).

The phenomenon that lamella thickness increases with the logarithm of time has been observed in many experiments (Fischer and Schmidt 1962; Wunderlich and Mielillo 1968). This continuous thickening of mobile high-molecular-weight polymer crystals was simulated by Monte Carlo simulations (Wang et al. 2012). Figure 4.29a demonstrates the wedge-shaped profile of the growth front resulted from the continuous thickening by chain-sliding diffusion at the growth front. Figure 4.29b provides three different growth-front profiles at different temperatures, which can be fitted into a logarithmic function of distances to the growth front. This function implies a logarithmic time dependence of crystal thickness. The prefactor in the function indicates an increasing thickening rate with increasing temperatures.

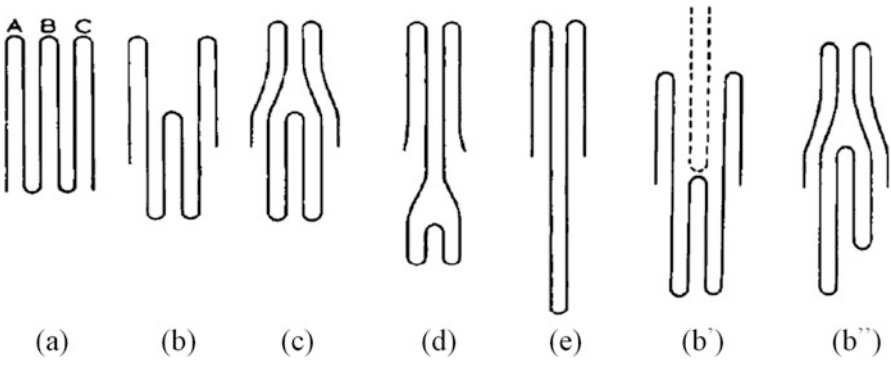

Fig. 4.28 Schematic picture of the fold-dislocation thickening model (Dreyfus and Keller 1970). (**a**) → (**e**) shows the thickening process of folded chain in a lamellar crystal. The space generated in this process should be filled by other stems (**b**′) or be discharged by merging of stems (**b**″)

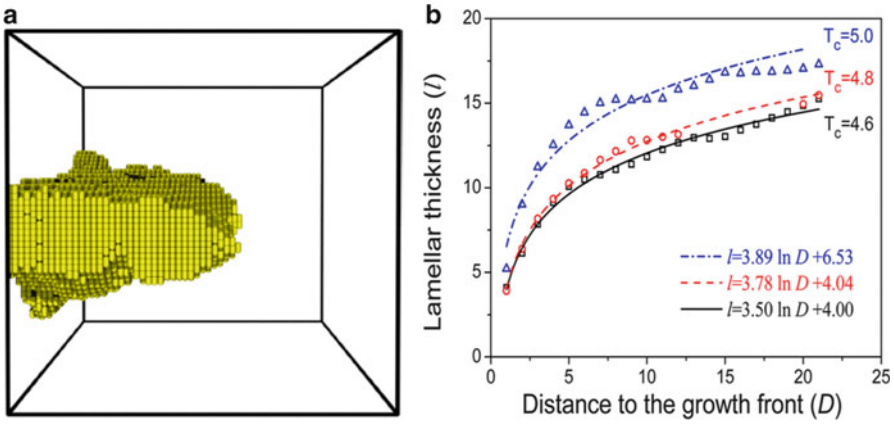

Fig. 4.29 (**a**) Snapshot of the wedge-shaped lamellar crystal of high-molecular-weight polymers grown for 35000MCc under $T = 4.6\,E_c/k_b$ in the 64^3 cubic lattice and polymer occupation density was 0.9375. Parameters were set as $E_p/E_c = 1$ for flexible chains and $E_f/E_c = 0.02$ to allow chain-sliding diffusion. The template was placed at the left end and only crystalline bonds were shown in *yellow color*. (**b**) Lamellar thickness as a function of distance to the growth front at three different temperatures $T = 4.6$, 4.8, and 5.0, respectively. The equations shown in the picture are the calculated logarithmic functions of distance D to the growth front (Wang et al. 2012)

This continuous thickening is obviously controlled by the chain-sliding diffusion in the crystals. The similar thickness profiles at the edges of lamellar polymer crystals have been observed in experiments (Reiter 2014).

The logarithmic-time dependence of crystal thickness can be deduced easily. By assuming a frictional barrier (ΔE_s) for chain-sliding diffusion proportional to the lamella thickness (l), thus the thickening rate of monolayer lamellar crystal under a certain temperature is

$$\frac{dl}{dt} \propto be^{-al/k_bT} \tag{4.76}$$

Equation (4.76) can be solved by

$$l = c \ln t + d \tag{4.77}$$

In the above equations, a, b, c, and d are the coefficients.

4.4 Summary

We made a brief introduction about our current theoretical models of thermodynamics and kinetics of polymer crystallization. We first introduced basic thermodynamic concepts, including the melting point, the phase diagram, the metastable state, and the mesophase. The mean-field statistical thermodynamics based on a

classic lattice model of polymer solutions, and its predictions on the melting points and phase diagrams were emphasized. Those molecular factors governing the melting points were also introduced. We then introduced crystal nucleation, crystal growth, and crystal annealing as the three basic stages of polymer crystallization. The classical nucleation theory as well as some recent ideas about primary nucleation were emphasized. On crystal growth, we introduced the secondary nucleation model, in particular, the well-known Lauritzen–Hoffman theory. The recently developed intramolecular nucleation model can be regarded as an updated version of secondary nucleation models. Some other models based on non-nucleation ideas were also introduced in a balanced way. The kinetics of crystal thickening, which is usually dominating crystal annealing, was also introduced under three typical circumstances.

Due to the length limitation, we have to skip many other theoretical aspects of polymer crystallization. We hope that our selected content above has already been strong enough to demonstrate the power of theoretical approaches, as a complemental to experimental approaches to gain a better understanding of the complicated polymer crystal morphologies.

References

Abo El Maaty MI, Bassett MD (2005) Evidence for isothermal lamellar thickening at and behind the growth front as polyethylene crystallizes from the melt. Polymer 46(20):8682–8688

Allegra G (1977) Chain folding and polymer crystallization: a statistical–mechanical approach. J Chem Phys 66(12):5453–5463

Allegra G (1980) Polymer crystallization: the bundle model. Ferroelectrics 30(1):195–211

Allegra G, Meille SV (1999) The bundle theory for polymer crystallisation. Phys Chem Chem Phys 1(22):5179–5188

Allegra G, Meille SV (2005) Pre-crystalline, high-entropy aggregates: a role in polymer crystallization? Adv Polym Sci 191:87–135

Arlie JP, Spegt PA, Skoulios AE (1966) Etude de la cristallisation des polymères I. Structure lamellaire de polyoxyéthylènes de faible masse moléculaire. Die Makromolekulare Chemie 99 (1):160–174

Arlie JP, Spegt PA, Skoulios AE (1967) Etude de la cristallisation des polymères. II. Structure lamellaire et repliement des chaines du polyoxyéthylène. Die Makromolekulare Chemie 104 (1):212–229

Armistead K, Goldbeck-Wood G (1992) Polymer crystallization theories. Adv Polym Sci 100:219–312

Becker R, Döring W (1935) Kinetische behandlung der keimbildung in übersättigten dämpfen. Ann Phys 416(8):719–752

Blundell D, Keller A, Kovacs A (1966) A new self-nucleation phenomenon and its application to the growing of polymer crystals from solution. J Polym Sci B Polym Lett 4(7):481–486

Burnett BB, Mcdevit W (1957) Kinetics of spherulite growth in high polymers. J Appl Phys 28 (10):1101–1105

Cai T, Ma Y, Yin P, Hu W (2008) Understanding the growth rates of polymer co-crystallization in the binary mixtures of different chain lengths. J Phys Chem B 112(25):7370–7376

Chang TS (1939) Statistical theory of absorption of double molecules. Proc R Soc Ser A 169 (939):512–531

Cheng SZ (2008) Phase transitions in polymers: the role of metastable states. Elsevier Science, Oxford
Cheng SZ, Wunderlich B (1986) Molecular segregation and nucleation of poly (ethylene oxide) crystallized from the melt. I. Calorimetric study. J Polym Sci B 24(3):577–594
Coleman BD (1958) On the properties of polymers with random stereo-sequences. J Polym Sci 31 (122):155–164
Colson JP, Eby RK (1966) Melting temperatures of copolymers. J Appl Phys 37(9):3511–3514
Dreyfus P, Keller A (1970) A simple chain refolding scheme for the annealing behavior of polymer crystals. J Polym Sci B Polym Lett 8(4):253–258
Fischer E (1969) Zusammenhänge zwischen der Kolloidstruktur kristalliner Hochpolymerer und ihrem Schmelz-und Rekristallisationsverhalten. Kolloid-Zeitschrift und Zeitschrift für Polymere 231(1-2):458–503
Fischer E, Schmidt G (1962) Long periods in drawn polyethylene. Angew Chem Int Ed Engl 1 (9):488–499
Flory PJ (1941) Thermodynamics of high polymer solutions. J Chem Phys 9(8):660
Flory PJ (1942) Thermodynamics of high polymer solutions. J Chem Phys 10(1):51–61
Flory PJ (1953) Principles of polymer chemistry. Cornell University Press, Ithaca
Flory PJ (1955) Theory of crystallization in copolymers. Trans Faraday Soc 51:848–857
Flory PJ (1956) Statistical thermodynamics of semi-flexible chain molecules. Proc R Soc Lond A Math Phys Sci 234(1196):60–73
Flory PJ (1962) On the morphology of the crystalline state in polymers. J Am Chem Soc 84 (15):2857–2867
Flory P, McIntyre A (1955) Mechanism of crystallization in polymers. J Polym Sci 18 (90):592–594
Flory P, Vrij A (1963) Melting points of linear-chain homologs. The normal paraffin hydrocarbons. J Am Chem Soc 85(22):3548–3553
Gee RH, Lacevic N, Fried LE (2005) Atomistic simulations of spinodal phase separation preceding polymer crystallization. Nat Mater 5(1):39–43
Gupta AM, Edwards SF (1993) Mean-field theory of phase transitions in liquid-crystalline polymers. J Chem Phys 98(2):1588–1596
Guth E, Mark H (1934) Zur innermolekularen statistik, insbesondere bei Ketten-molekiilen I. Monatshefte für Chemie/Chemical Monthly 65(1):93–121
Heeley E, Maidens A, Olmsted P, Bras W, Dolbnya I, Fairclough J, Terrill N, Ryan A (2003) Early stages of crystallization in isotactic polypropylene. Macromolecules 36(10):3656–3665
Hermann K, Gerngross O (1932) Die elastizitat des kautschuks. Kautschuk 8:181
Hermann K, Gerngross O, Abitz W (1930) Zur rontgenographischen strukturforschung des gelatinemicells. Zeitschrift für Physikalische Chemie B 10:371–394
Hikosaka M (1987) Unified theory of nucleation of folded-chain crystals and extended-chain crystals of linear-chain polymers. Polymer 28(8):1257–1264
Hikosaka M (1990) Unified theory of nucleation of folded-chain crystals (FCCs) and extended-chain crystals (ECCs) of linear-chain polymers: 2. Origin of FCC and ECC. Polymer 31 (3):458–468
Hikosaka M, Okada H, Toda A, Rastogi S, Keller A (1995) Dependence of the lamellar thickness of an extended-chain single crystal of polyethylene on the degree of supercooling and the pressure. J Chem Soc Faraday Trans 91(16):2573–2579
Hoffman JD (1983) Regime III crystallization in melt-crystallized polymers: the variable cluster model of chain folding. Polymer 24(1):3–26
Hoffman JD, Lauritzen J (1961) Crystallization of bulk polymers with chain folding: theory of growth of lamellar spherulites. J Res Natl Bur Stand A65(4):297–336
Hoffman JD, Miller RL (1997) Kinetic of crystallization from the melt and chain folding in polyethylene fractions revisited: theory and experiment. Polymer 38(13):3151–3212
Hoffman JD, Weeks JJ (1965) X-Ray study of isothermal thickening of lamellae in bulk polyethylene at the crystallization temperature. J Chem Phys 42(12):4301–4302

Hoffman JD, Davis GT, Lauritzen JI Jr (1976) The rate of crystallization of linear polymers with chain folding. In: Hannay NB (ed) Treatise on solid state chemistry, vol 3. Plenum Press, New York

Holland V, Lindenmeyer P (1962) Morphology and crystal growth rate of polyethylene crystalline complexes. J Polym Sci 57(165):589–608

Hu W (1998) Structural transformation in the collapse transition of the single flexible homopolymer model. J Chem Phys 109(9):3686–3690

Hu W (2000) The melting point of chain polymers. J Chem Phys 113(9):3901–3908

Hu W (2005) Molecular segregation in polymer melt crystallization: simulation evidence and unified-scheme interpretation. Macromolecules 38(21):8712–8718

Hu W (2007) Intramolecular crystal nucleation. In: Reiter G, Strobl GR (eds) Lecture notes in physics: progress in understanding of polymer crystallization. Springer, Berlin, pp 47–63

Hu W (2013) Polymer physics: a molecular approach. Springer, Wien

Hu W, Cai T (2008) Regime transitions of polymer crystal growth rates: molecular simulations and interpretation beyond Lauritzen-Hoffman model. Macromolecules 41(6):2049–2061

Hu W, Frenkel D (2004) Effect of metastable liquid-liquid demixing on the morphology of nucleated polymer crystals. Macromolecules 37(12):4336–4338

Hu W, Frenkel D (2005) Polymer crystallization driven by anisotropic interactions. Adv Polym Sci 191:1–35

Hu W, Frenkel D, Mathot VB (2003a) Lattice-model study of the thermodynamic interplay of polymer crystallization and liquid–liquid demixing. J Chem Phys 118(22):10343–10348

Hu W, Frenkel D, Mathot VB (2003b) Intramolecular nucleation model for polymer crystallization. Macromolecules 36(21):8178–8183

Hu W, Frenkel D, Mathot VB (2003c) Sectorization of a lamellar polymer crystal studied by dynamic Monte Carlo simulations. Macromolecules 36(3):549–552

Huggins ML (1942) Thermodynamic properties of solutions of long-chain compounds. Ann N Y Acad Sci 43:1–32

Imai M, Kaji K, Kanaya T (1993) Orientation fluctuations of poly (ethylene terephthalate) during the induction period of crystallization. Phys Rev Lett 71(25):4162–4165

Imai M, Kaji K, Kanaya T (1994) Structural formation of poly (ethylene terephthalate) during the induction period of crystallization. 3. Evolution of density fluctuations to lamellar crystal. Macromolecules 27(24):7103–7108

Jähnig F (1979) Molecular theory of lipid membrane order. J Chem Phys 70(7):3279–3290

Jiang X, Li T, Hu W (2015) Understanding the growth rates of polymer co-crystallization in the binary mixtures of different chain lengths: Revisited. J Phys Chem B 119(30):9975–9981

Jiang X, Reiter G, Hu W (2016) How chain-folding crystal growth determines thermodynamic stability of polymer crystals. J Phys Chem B 120(3):566–571

Keller A (1957) A note on single crystals in polymers: evidence for a folded chain configuration. Philos Mag 2(21):1171–1175

Keller A (1992) Morphology of polymers. Pure Appl Chem 64(2):193–204

Keller A, Hikosaka M, Rastogi S, Toda A, Barham P, Goldbeck-Wood G, Windle A, Thomas E, Bassett D (1994) The size factor in phase transitions: its role in polymer crystal formation and wider implications [and discussion]. Philos Trans R Soc Lond Ser A Phys Eng Sci 348 (1686):3–17

Kelton K (1991) Crystal nucleation in liquids and glasses. Solid State Phys 45:75–177

Khokhlov A, Semenov A (1985) On the theory of liquid-crystalline ordering of polymer chains with limited flexibility. J Stat Phys 38(1–2):161–182

Kraack H, Sirota E, Deutsch M (2000) Measurements of homogeneous nucleation in normal-alkanes. J Chem Phys 112(15):6873–6885

Kuhn W (1934) Über die gestalt fadenförmiger moleküle in lösungen. Kolloid-Zeitschrift 68 (1):2–15

Lauritzen JI, Hoffman JD (1960) Theory of formation of polymer crystals with folded chains in dilute solution. J Res Natl Bur Stand A Phys Chem 64(1):73–102

Lekkerkerker H, Vroege G (1993) Lyotropic colloidal and macromolecular liquid crystals. Philos Trans R Soc Lond Ser A Phys Eng Sci 344(1672):419–440
Ma Y, Hu W, Wang H (2007) Polymer immiscibility enhanced by thermal fluctuations toward crystalline order. Phys Rev E 76(3):031801
Ma Y, Zha L, Hu W, Reiter G, Han CC (2008) Crystal nucleation enhanced at the diffuse interface of immiscible polymer blends. Phys Rev E 77(6):061801
Maier W, Saupe A (1959) A simple molecular statistical theory of the nematic crystalline-liquid phase. Zeitschrift für Naturforschung 14:882–889
Mandelkern L (1964) Crystallization of polymers. McGraw-Hill, New York
Matsuoka S (1962) The effect of pressure and temperature on the specific volume of polyethylene. J Polym Sci 57(165):569–588
Mehta A, Wunderlich B (1975) A study of molecular fractionation during the crystallization of polymers. Colloid Polym Sci 253(3):193–205
Metropolis N, Rosenbluth AW, Rosenbluth MN, Teller AH, Teller E (1953) Equation of state calculations by fast computing machines. J Chem Phys 21(6):1087–1092
Meyer K (1939) The compound entropies of systems with long-chain compounds and their statistical explanation. Zeitschrift für Physikalische Chemie B 44:383–391
Milner ST (2011) Polymer crystal-melt interfaces and nucleation in polyethylene. Soft Matter 7:2909–2917
Mullin N, Hobbs JK (2011) Direct imaging of polyethylene films at single-chain resolution with torsional tapping atomic force microscopy. Phys Rev Lett 107(19):197801
Muthukumar M (2005) Modeling polymer crystallization. Adv Polym Sci 191:241–274
Nie Y, Gao H, Ma Y, Hu Z, Reiter G, Hu W (2013) Competition of crystal nucleation to fabricate the oriented semi-crystalline polymers. Polymer 54(13):3402–3407
Olley R, Bassett D (1977) Molecular conformations in polyethylene after recrystallization or annealing at high pressures. J Polym Sci Polym Phys Ed 15(6):1011–1027
Olmsted PD, Poon WC, Mcleish T, Terrill N, Ryan A (1998) Spinodal-assisted crystallization in polymer melts. Phys Rev Lett 81(2):373–376
Onsager L (1949) The effects of shape on the interaction of colloidal particles. Ann N Y Acad Sci 51(4):627–659
Organ SJ, Keller A (1987) The onset of chain folding in ultralong n-alkanes: an electron microscopic study of solution-grown crystals. J Polym Sci B 25(12):2409–2430
Peterlin A (1963) Thickening of polymer single crystals during annealing. J Polym Sci B Polym Lett 1(6):279–284
Prasad A, Mandelkern L (1989) Equilibrium dissolution temperature of low molecular weight polyethylene fractions in dilute solution. Macromolecules 22(12):914–920
Prigogine I (1957) The molecular theory of solution. North-Holland, Amsterdam
Prime RB, Wunderlich B (1969) Extended-chain crystals. III. Size distribution of polyethylene crystals grown under elevated pressure. J Polym Sci A2 Polym Phys 7(12):2061–2072
Reiter G (2014) Some unique features of polymer crystallization. Chem Soc Rev 43:2055–2065
Ren Y, Ma A, Li J, Jiang X, Ma Y, Toda A, Hu W (2010) Melting of polymer single crystals studied by dynamic Monte Carlo simulations. Eur Phys J E 33(3):189–202
Ronca G, Yoon D (1982) Theory of nematic systems of semiflexible polymers. I. High molecular weight limit. J Chem Phys 76(6):3295–3299
Ronca G, Yoon D (1984) Theory of nematic systems of semiflexible polymers. II. Chains of finite length in the bulk. J Chem Phys 80(2):925–929
Sadler DM, Gilmer GH (1988) Selection of lamellar thickness in polymer crystal growth: a rate-theory model. Phys Rev B 38(8):5684–5693
Sadler DM, Barber M, Lark G, Hill MJ (1986) Twin morphology: 2. Measurements of the enhancement in growth due to re-entrant corners. Polymer 27(1):25–33
Sanchez I, Eby R (1975) Thermodynamics and crystallization of random copolymers. Macromolecules 8(5):638–641

Sanchez I, Colson J, Eby R (1973) Theory and observations of polymer crystal thickening. J Appl Phys 44(10):4332–4339
Sanchez I, Peterlin A, Eby R, Mccrakin F (1974) Theory of polymer crystal thickening during annealing. J Appl Phys 45(10):4216–4219
Sirota E (2000) Supercooling and transient phase induced nucleation in n-alkane solutions. J Chem Phys 112(1):492–500
Sirota E, Herhold A (1999) Transient phase-induced nucleation. Science 283(5401):529–532
Spells SJ, Sadler DM, Keller A (1980) Chain trajectory in solution grown polyethylene crystals: correlation between infra-red spectroscopy and small-angle neutron scattering. Polymer 21 (10):1121–1128
Strobl G (2000) From the melt via mesomorphic and granular crystalline layers to lamellar crystallites: a major route followed in polymer crystallization? Eur Phys J E 3(2):165–183
Strobl G (2005) A thermodynamic multiphase scheme treating polymer crystallization and melting. Eur Phys J E 18(3):295–309
Strobl G (2006) Crystallization and melting of bulk polymers: new observations, conclusions and a thermodynamic scheme. Prog Polym Sci 31(4):398–442
Strobl G (2009) Colloquium: laws controlling crystallization and melting in bulk polymers. Rev Mod Phys 81(3):1287–1300
ten Bosch A, Maissa AP, Sixou P (1983a) Molecular model for nematic polymers in liquid crystal solvents. J Chem Phys 79(7):3462–3466
ten Bosch A, Maissa AP, Sixou P (1983b) A Landau-de Gennes theory of nematic polymers. J Phys Lett 44(3):105–111
Terrill NJ, Fairclough PA, Towns-Andrews E, Komanschek BU, Young RJ, Ryan AJ (1998) Density fluctuations: the nucleation event in isotactic polypropylene crystallization. Polymer 39(11):2381–2385
Turnbull D, Fisher JC (1949) Rate of nucleation in condensed systems. J Chem Phys 17(1):71–73
Ungar G, Stejny J, Keller A, Bidd I, Whiting M (1985) The crystallization of ultralong normal paraffins: the onset of chain folding. Science 229(4711):386–389
Volmer M, Weber A (1926) Nucleus formation in supersaturated systems. Zeitschrift für Physikalische Chemie 119:277–301
Wang H (2006) SANS study of the early stages of crystallization in polyethylene solutions. Polymer 47(14):4897–4900
Wang ZG, Hsiao BS, Sirota EB, Agarwal P, Srinivas S (2000) Probing the early stages of melt crystallization in polypropylene by simultaneous small-and wide-angle X-ray scattering and laser light scattering. Macromolecules 33(3):978–989
Wang M, Gao H, Zha L, Chen EQ, Hu W (2012) Systematic kinetic analysis on monolayer lamellar crystal thickening via chain-sliding diffusion of polymers. Macromolecules 46 (1):164–171
Welch P, Muthukumar M (2001) Molecular mechanisms of polymer crystallization from solution. Phys Rev Lett 87(21):218302
Wunderlich B (1976) Macromolecular physics. 2. Crystal nucleation, growth, annealing. Academic, New York
Wunderlich B (1979) Molecular nucleation and segregation. Faraday Discuss Chem Soc 68:239–243
Wunderlich B (2003) Reversible crystallization and the rigid–amorphous phase in semicrystalline macromolecules. Prog Polym Sci 28(3):383–450
Wunderlich B (2005) Thermal analysis of polymeric materials. Springer, Berlin
Wunderlich B, Cormier C (1966) Seeding of supercooled polyethylene with extended chain crystals. J Phys Chem 70(6):1844–1849
Wunderlich B, Mehta A (1974) Macromolecular nucleation. J Polym Sci Polym Phys Ed 12 (2):255–263
Wunderlich B, Mielillo L (1968) Morphology and growth of extended chain crystals of polyethylene. Die Makromolekulare Chemie 118(1):250–264

Wunderlich B, Melillo L, Cormier C, Davidson T, Snyder G (1967) Surface melting and crystallization of polyethylene. J Macromol Sci B Phys 1(3):485–516

Zachmann H (1967) Der einfluss der konfigurationsentropie auf das kristallisations und schmelzverhalten von hochpolymeren stoffen. Kolloid-Zeitschrift und Zeitschrift für Polymere 216–217(1):180–191

Zachmann H (1969) Statistische thermodynamik des kristallisierens und schmelzens von hochpolymeren stoffen. Colloid Polym Sci 231(1):504–534

Zhang J, Muthukumar M (2007) Monte Carlo simulations of single crystals from polymer solutions. J Chem Phys 126(23):234904–234921